https://doi.org/10.5194/bg-2020-201
Preprint. Discussion started: 18 June 2020

Biogeosciences Discussions

Variability of the Surface Energy Balance in Permafrost Underlain Boreal Forest

Simone Maria Stuenzi[1,2], Julia Boike[1,2], William Cable[1], Ulrike Herzschuh[1,3], Stefan Kruse[1,3], Ljudmila Pestryakova[5], Thomas Schneider v. Deimling[1], Sebastian Westermann[6], Evgenii Zakharov[4,5], and Moritz Langer[1,2]

[1]Alfred Wegener Institute Helmholtz Centre for Polar and Marine Research, Telegrafenberg A45, 14473 Potsdam, Germany
[2]Humboldt Universität zu Berlin, Geography Department, Unter den Linden 6, 10099 Berlin, Germany
[3]Institute of Earth and Environmental Science, University of Potsdam, 14476 Potsdam-Golm, Germany
[4]Institute for Biological Problems of Cryolithozone Siberian Branch of RAS, Yakutsk, Russian Federation
[5]Federal State Autonomous Educational Institution of Higher Education "M.K. Ammosov North-Eastern Federal University", Yakutsk, Russian Federation
[6]University of Oslo, Department of Geosciences, Sem Sælands vei 1, 0316 Oslo, Norway

Correspondence: Simone Maria Stuenzi (simone.stuenzi@awi.de)

Abstract. Boreal forests in permafrost regions make up around one-third of the global forest cover and are an essential component of regional and global climate patterns. Further, climatic change can trigger extensive ecosystem shifts such as the partial disappearance of near surface permafrost or changes to the vegetation structure and composition. Therefore, our aim is to understand how the interactions between the vegetation, permafrost, and the atmosphere stabilize the forests and the underlying permafrost. Existing model set-ups are often static or are not able to capture important processes such as the vertical structure or the leaf physiological properties. There is a need for a physically based model with a robust radiative transfer scheme through the canopy. A one-dimensional land surface model (CryoGrid) is adapted for the application in vegetated areas by coupling a multilayer canopy model (CLM-ml v0) and is used to reproduce the energy transfer and thermal regime at a study site (N 63.18946°, E 118.19596°) in mixed boreal forest in Eastern Siberia. We have in-situ soil temperature and radiation measurements, to evaluate the model and demonstrate the capabilities of a coupled multilayer forest-permafrost model to investigate the vertical exchange of radiation, heat, and water. We find that the forests exert a strong control on the thermal state of permafrost through changing the radiation balance and snow cover phenology. The forest cover alters the surface energy balance by inhibiting over 90% of the solar radiation and suppressing turbulent heat fluxes. Additionally, our simulations reveal a surplus in longwave radiation trapped below the canopy, similar to a greenhouse, which leads to a comparable magnitude in storage heat flux to that simulated at the grassland site. Further, the end of season snow cover is three times greater at the forest site and the onset of the snow melting processes are delayed.

https://doi.org/10.5194/bg-2020-201
Preprint. Discussion started: 18 June 2020

Biogeosciences Discussions

1 Introduction

Around 80% of the world's boreal forest occurs in the circumpolar permafrost zone (Helbig et al., 2016). Despite little human interference, and due to extreme climate conditions such as winter temperatures below $-50\,^{\circ}\mathrm{C}$ and very low precipitation, the biome is highly sensitive to climatic changes (ACIA, 2005; AMAP, 2011; IPCC, 2014) and thus prone to vegetation shifts. Boreal forest regions are expected to warm by 4 to $11\,^{\circ}\mathrm{C}$ by 2100, coupled with a more modest precipitation increase (IPCC, 2014; Scheffer et al., 2012). Moreover, during 2007-2016 continuous zone permafrost temperatures have increased by $0.39\ (\pm 0.15)\,^{\circ}\mathrm{C}$ (Biskaborn et al., 2019; IPCC, 2019). The northeastern part of the Eurasian continent is dominated by such vast boreal forest - the taiga. Due to its sheer size, the biome is not only sensitive to climatic changes, but also exerts a strong control on numerous climate feedback mechanisms through the altering of land-surface reflectivity, the emission of biogenic volatile organic compounds and greenhouse gases, and the transfer of water to the atmosphere (Bonan et al., 2018; Zhang et al., 2011). The forests are usually considered to efficiently insulate the underlying permafrost (Chang et al., 2015). The canopy exerts shading by reflecting and absorbing most of the downward solar radiation, changes the surface albedo and decreases the soil moisture by intercepting precipitation and increasing evapotranspiration (Vitt et al., 2000). Additionally, the forest promotes the accumulation of an organic surface layer which further insulates the soil from the atmosphere (Bonan and Shugart, 1989). Changing climatic conditions can promote an increasing active layer depth or trigger the partial disappearance of the near surface permafrost. Further, extensive ecosystem shifts such as a change in composition, density or the distribution of vegetation have already been reported (Holtmeier and Broll, 2005; Pearson et al., 2013; Gauthier et al., 2015; Kruse et al., 2016; Ju and Masek, 2016). Changes to the vegetation - permafrost dynamics can have a potentially high impact on the numerous feedback mechanisms between the two ecosystem components, which can then trigger biogeochemical processes that could potentially release large amounts of carbon to the atmosphere (Schneider Von Deimling et al., 2012; Romanovsky et al., 2017).

These vegetation - permafrost dynamics in Eastern Siberia have been documented through exploratory and descriptive field studies showing a clear insulation effect of forests on soil temperatures (Chang et al., 2015). Further, the biogeophysical processes controlling the evolution of the ecosystem have been described by conceptual models (Beer et al., 2007; Zhang et al., 2011; Sato et al., 2016). Modeling schemes such as Orchidee-Can (Chen et al., 2016), JULES (Chadburn et al., 2015), Lund-Potsdam-Jena (LPJ DGVM) (Beer et al., 2007), NEST (Zhang et al., 2003) or SiBCliM (Tchebakova et al., 2009), have added a vegetation or canopy module, with defined exchange coefficients for the fluxes of mass and energy, to their soil modules. This is feasible to varying levels of complexity and the models are capable of addressing a variety of different aspects such as forest establishment and mortality (Sato et al., 2016), unfrozen vs. frozen ground and fire disturbances (Zhang et al., 2011) or the evolution of the vegetation carbon density under diverse warming scenarios (Beer et al., 2007).

While all of these studies have significantly improved our understanding of essential mechanisms in boreal permafrost ecosystems, it is important to further understand how a forest canopy affects the thermal state and the snow regime of the ground, especially amid ongoing shifts in forest composition (Loranty et al., 2018). The existing model set-ups are often static or not able to capture important processes such as the vertical canopy structure or the leaf physiological properties which

https://doi.org/10.5194/bg-2020-201
Preprint. Discussion started: 18 June 2020


Biogeosciences Discussions Open Access EGU

determine the energy transfer between the top of the canopy atmosphere and the ground. Therefore, there is a need for a physically based model with a robust radiative transfer scheme through the canopy for a detailed analysis of the vegetation's impact on the hydro-thermal regime of the permafrost ground below.

With a tailored version of a one-dimensional land surface model (CryoGrid, Westermann et al. (2016)) we perform and analyze numerical simulations and reproduce the energy transfer and surface energy balance in permafrost underlain boreal forest of Eastern Siberia. CryoGrid has, so far, not included a vegetation scheme but has been used to successfully describe atmosphere-ground energy transfer and the ground thermal regime in barren and grass-covered areas (Langer et al., 2016; Westermann et al., 2016; Nitzbon et al., 2019, 2020). In our study, we have adapted a state-of-the-art multilayer vegetation model (CLM-ml v0, originally developed for the Community Land Model CLM by Bonan et al. (2018)). We tailor and implement this scheme to simulate the turnover of heat, water, and snow between atmosphere, forest canopy and ground. We take advantage of a detailed in-situ data record from a study site, which is used to provide model parameters, as well as for model validation by comparing field measurements with simulation results. The main objectives of this study are

1. To demonstrate the capabilities of a coupled multilayer forest - permafrost model to simulate vertical exchange of radiation, heat, and water for boreal forests.

2. To investigate the impact of the detailed canopy module on the surface energy balance of the underlying permafrost at a mixed boreal forest site in Eastern Siberia.

2 Methods

2.1 Study Area

The study site is located south east of Nyurba (N $63.18946°$, E $118.19596°$) in a typical boreal forest zone intermixed with some grassland for horse grazing and shallow lakes. The forest is rather dense and mixed, with the dominant taxa evergreen spruce (*Picea obovata*, 92%), deciduous larch (*Larix gmelinii*, 7.3%) and some hardwood birch (*Betula pendula*, <1%). The average tree height is $5.5\,\mathrm{m}$ for spruce and $12\,\mathrm{m}$, respectively. These boreal forest environments experience 6 to 8 months of freezing temperatures reaching extremes of $-62\,^{\circ}\mathrm{C}$ in winter and up to $35\,^{\circ}\mathrm{C}$ between May and September. The low annual average temperatures result in continuous permafrost and therefore poorly drained, podzolized and nutrient-poor soils (Chapin et al., 2011). The summer precipitation has decreased over the past 30 years (Hayasaka, 2011). The temperature trend from 1970 to 2010 for the Central Yakutian region is positive for spring, summer and fall and negative for winter (monthly surface temperature quantified using Climatic Research Unit (CRU) TS4.01 data (Harris et al., 2014; Stuenzi and Schaepman-Strub, 2020)). The treeline of Northern Siberia is dominated by the deciduous needleleaf tree genus *Larix* Mill. up to N $72.08°$. *Larix sibirica* Ledeb. from E $60-90°$, *Larix gmelinii* Rupr. between E $90-120°$ and *Larix cajanderi* Mayr. from E $120-160°$ (see Fig. 1). Larch compete effectively with other tree taxa because of its deciduous leaf habit and dense bark. In more southern margins of Eastern Siberia, such as our study area, larch is mixed with evergreen conifers (Siberian pine (*Pinus sibirica, Pinus sylvestris*), spruce (*Picea obovata Ledeb.*), and fir (*Abies sibirica*)), and hardwood (*Betula pendula Roth., B. pubescence Ehrh.,*

https://doi.org/10.5194/bg-2020-201
Preprint. Discussion started: 18 June 2020

Biogeosciences Discussions
Open Access
EGU

Populus tremula L.) (Kharuk et al., 2019). Moreover, the ground vegetation is poor in diversity and dominated by mosses and lichens that form carpets. Larch has shallow roots, and grows on clay permafrost soils with an active layer of around $0.7\,\mathrm{m}$ and a maximum wetness of 20-40 %. Evergreen conifers and hardwood both prefer deeper active layers and a higher soil moisture availability (Ohta et al., 2001; Furyaev et al., 2001; Rogers et al., 2015).

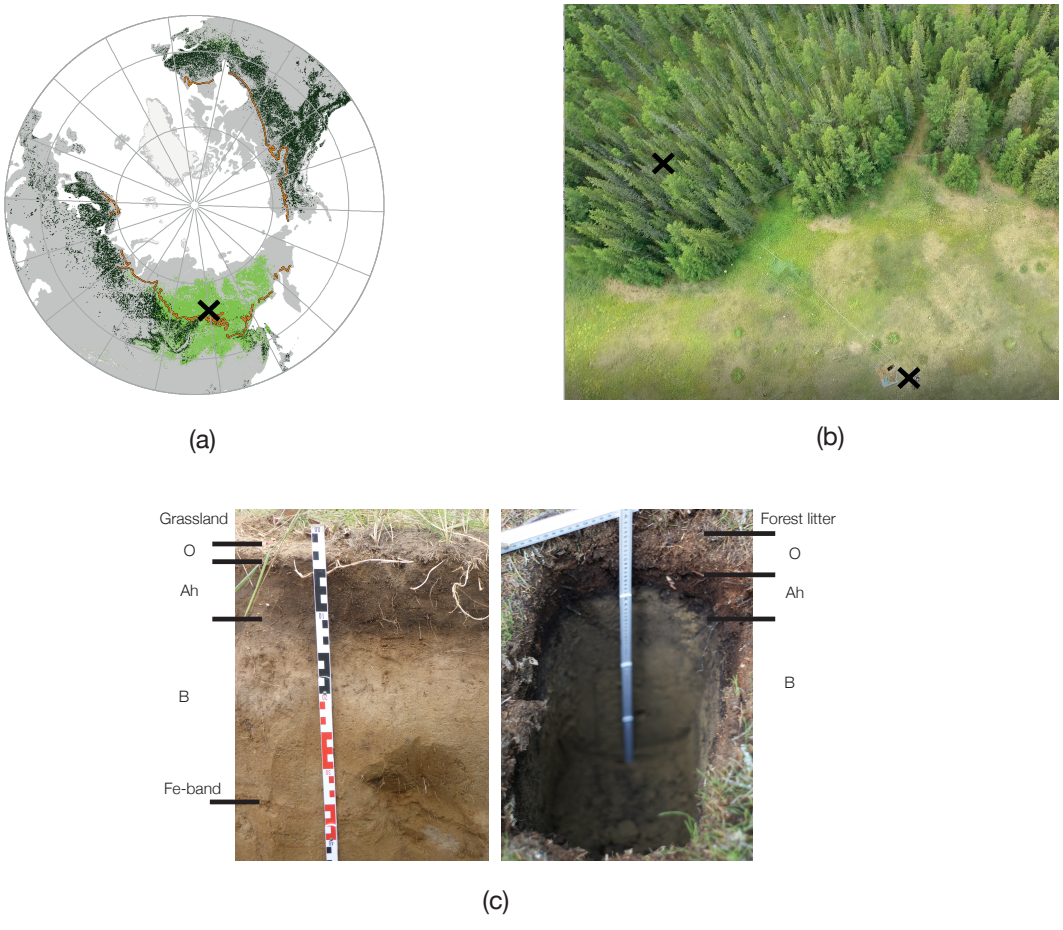

Figure 1. (a) Global evergreen needleleaf (dark green) and summergreen needleleaf (light green) boreal forest distribution and the boundary line between the discontinuous and continuous permafrost extent in brown. The study site is marked with a black cross. Data: ESA CCI Land Cover forest classes. ESA. Land Cover CCI Product User Guide Version 2. Tech. Rep. (2017). (b) Overview image of the location of the meteorological station in the grassland in the lower right corner and the location of the instrumented forest site in the upper left corner. (c) Respective soil profiles with the depths of the organic matter dominated O horizon, the top layer of the mineral soil containing the decomposed organic layer (Ah horizon) and the subsoil mineral layer (B horizon) at the grassland site (left) and at the forest site (right).

https://doi.org/10.5194/bg-2020-201
Preprint. Discussion started: 18 June 2020


Biogeosciences Discussions Open Access EGU

2.2 Meteorological and soil physical measurements

An automatic weather station (AWS, Campbell Scientific, detailed list of sensors see Table A1) is installed at $110\,\mathrm{m\,a.s.l.}$ on a meadow next to the forest patch described above. The grassland is grazed by horses in summer and deforestation occurred more then 50 years ago. The AWS records air temperature and relative humidity at two heights ($1.1\,\mathrm{m}$ and $2.5\,\mathrm{m}$) above the ground while wind speed and direction are measured at $3.2\,\mathrm{m}$ above ground. In addition, the station measures liquid precipitation, snow depth, incoming and outgoing short and longwave radiation and is equipped as a Bowen Ratio station (B, see Appendix A). All meteorological variables were recorded with 10 min resolution and stored as 30 min averages. In order to install soil temperature and moisture sensors in the ground a soil pit was excavated in immediate vicinity ($2.5\,\mathrm{m}$) of the AWS. The O horizon has a depth of $0.04\,\mathrm{m}$, the A horizon $0.1\,\mathrm{m}$ containing undecomposed roots, dead moss remains, dense rooting and some organic hummus. The mineral soil is podsolized, sandy and dominated by quartz. The rooting depth is $0.18\,\mathrm{m}$. Iron rich bands were found at $0.4\,\mathrm{m}$, $0.7\,\mathrm{m}$ and $1.1\,\mathrm{m}$. The active layer thickness was $2.3\,\mathrm{m}$ in mid-August 2018 and in early-August 2019. In this soil pit, soil temperature and moisture measurement profiles are installed from the top to the bottom of the active layer consisting of 8 temperature sensors ($0.07\,\mathrm{m}, 0.26\,\mathrm{m}, 0.88\,\mathrm{m}, 1.33\,\mathrm{m}, 1.28\,\mathrm{m}, 1.58\,\mathrm{m}, 1.98\,\mathrm{m}, 2.28\,\mathrm{m}$) and 4 moisture probes ($0.07\,\mathrm{m}, 0.26\,\mathrm{m}, 0.88\,\mathrm{m}, 1.33\,\mathrm{m}$). In addition the conductive ground heat flux in the topsoil layer is measured with a heat flux plate installed at $0.02\,\mathrm{m}$ depth. Further, we record the near surface ground temperature with 5 standalone temperature loggers (iButtons, see Tab. A1) with a measurement interval of 3 hours. These are installed in the upper $0.03\,\mathrm{m}$ of the organic soil at our forest site. The forest soil has a litter layer of $0.08\,\mathrm{m}$ and an organic rich A-horizon reaching a depth of $0.16\,\mathrm{m}$. It is rich in organic and undecomposed material. Mineral soil is podsolized and the rooting depth is $0.20\,\mathrm{m}$. The average active layer thickness between spatially distributed point measurements was $0.75\,\mathrm{m}$ in mid-August 2018 and $0.73\,\mathrm{m}$ in early-August 2019. In a vegetation survey along a $150\,\mathrm{m}$ transect from the grassland into the forest, the tree height of every tree within a $2\,\mathrm{m}$ distance was estimated. Together, the instrumentation with a variety of different loggers, records the spatial and temporal variances across the two sites which are representative for a large area of the mixed boreal forest domain in Eastern Siberia (dataset in review: https://doi.org/10.1594/PANGAEA.914327).

2.3 Model description

2.3.1 Ground module

CryoGrid is a one-dimensional, numerical land surface model developed to simulate landscape processes related to permafrost such as surface subsidence, thermokarst, and ice wedge degradation. The model version is originally described in Westermann et al. (2016) and has since been extended with different functionalities such as lake heat transfer (Langer et al., 2016), multi-tiling (Nitzbon et al., 2019, 2020), and an extensive snow scheme based on CROCUS (Vionnet et al., 2012; Zweigel et al., 2020). The thermo-hydrological regime of the ground is simulated by numerically solving the one-dimensional heat equation with ground water phase change while ground water flow is simulated with an explicit bucket scheme (Nitzbon et al., 2019). The exchange of sensible and latent heat, radiation, evaporation, and condensation at the ground surface are simulated with an surface energy balance scheme based on atmospheric stability functions. In addition, the model encompasses different options

https://doi.org/10.5194/bg-2020-201
Preprint. Discussion started: 18 June 2020

to simulate the evolution of the snow cover including the Crocus snowpack scheme as implemented by Zweigel et al. (2020). The model is forced by standard meteorological variables which may be obtained from AWSs, reanalysis products, or climate models. The required forcing variables include air temperature, wind speed, humidity, incoming short-and longwave radiation, air pressure and precipitation (snow- and rainfall) (Westermann et al., 2016). The change of internal energy of the subsurface domain over time is controlled by fluxes across the upper and lower boundaries written as

$$\frac{\delta E}{\delta t} = S_{\mathrm{in}} - S_{\mathrm{out}} + L_{\mathrm{in}} - L_{\mathrm{out}} - Q_{\mathrm{h}} - Q_{\mathrm{e}} - Q_{\mathrm{h_{precip}}}, \quad (1)$$

where the input to the uppermost grid cell is derived from the fluxes of shortwave radiation (S_{in}, S_{out}) and longwave (L_{in}, L_{out}) radiation, at the same time regarding the latent (Q_e), sensible (Q_h), sensible heat added by precipitation (Q_{precip}) and storage heat flux (Q_s) between the atmosphere and the ground surface (Westermann et al., 2016).

For this study, we have adapted the multilayer canopy model developed by Bonan et al. (2014, 2018). The canopy model is coupled to CryoGrid by replacing its standard surface energy balance scheme while soil state variables are passed back to the forest module. In the following, we describe the canopy module and its interaction with the existing CryoGrid soil and snow scheme. All differences towards former CryoGrid parameterizations are summarized in Table 1.

Table 1. Overview of the processes for which this study differs from the former CG parameterizations.

Process / Parameter	CG	CG crocus + CLM-ml v0
Surface energy balance	*See Eq. 1*	*See Eq. 2, after Bonan et al. (2018)*
Precipitation interception	*Direct precipitation from forcing data Westermann et al. (2016)*	*Precipitation modulated by canopy interception. See Eq. 4, after Bonan (2019)*
Dynamic evapotranspiration	-	*See Eq. 7 in Bonan et al. (2018)*
Snow scheme	*See Westermann et al. (2016)*	*Crocus snow scheme. See sect. 2.3.3 after Zweigel et al. (2020)*

2.3.2 Canopy module

The multilayer canopy model provides a comprehensive parameterization of fluxes from the ground, through the canopy up to the roughness sublayer. The implementation of a roughness sublayer allows the representation of different forest canopy structures and their impact on the vertical heat and moisture transfer. The concept is similar to the multilayer approach in ORCHIDEE-CAN (Chen et al., 2016; Ryder et al., 2016). In an iterative manner, photosynthesis, leaf water potential, stomatal conductance, leaf temperature and leaf fluxes are calculated. This improves model performance in terms of capturing the stomatal conductance and canopy physiology, nighttime friction velocity and the diurnal radiative temperature cycle and sensible heat flux (Bonan et al., 2014, 2018).

https://doi.org/10.5194/bg-2020-201
Preprint. Discussion started: 18 June 2020

The multilayer canopy model (Bonan et al., 2018) was developed based on the use with CLM soil properties. Following the notations summarized in Bonan (2019) we developed a CLM-independent multilayer canopy module which can be coupled to CryoGrid by integrating novel interactions and an adapted snow cover parameterization. In order to set necessary parameters of the canopy module we make use of values defined for the plant functional type deciduous needleleaf forest of CLM. Please note that all parameters defining the canopy are set as constant values so that vegetation is not dynamic and changes in forest composition or actual tree growth are not considered in this study.

2.3.3 Snow module

The snow module employed in this study is based on Zweigel et al. (2020) (submitted, available upon request). Zweigel et al. (2020) extend the CryoGrid model with a snow microphysics parameterizations based on the CROCUS snow scheme (Vionnet et al., 2012), as well as lateral snow redistribution. The CLM-ml (v0) multilayer canopy model has not yet been coupled to a snow scheme (Bonan et al., 2018). Following Vionnet et al. (2012) the microstructure of the snow pack is characterized by grain size (gs, mm), sphericity (s, unitless, range 0-1), and dendricity (d, unitless, range 0-1). Fresh snow is added on top of the existing snow layers with temperature and windspeed dependent density and properties. After deposition the development of each layers microstructure occurs based on temperature gradients and liquid water content (Vionnet et al., 2012). Snow albedo for the surface layer and an absorption coefficient for each layer are calculated based on the snow properties. Solar radiation is gradually absorbed throughout the snow layers and the remaining radiation is added to the lowest cell. Additionally, the two mechanical processes of mechanical settling due to overload pressure and wind compression increase snow density and compaction. During snowfall, new snow is added to the top layer in each timestep and mixed with the old snow based on the amount of ice. Once a cell exceeds the snow water equivalent of $0.01\,\mathrm{m}$, which equals a snow layer thickness of $0.03\,\mathrm{m}$, a new snow layer is built. Here, snow accumulates on the ground under the forest canopy. During the first snowfall, the surface energy balance of the ground and snow is calculated for each respective cover fraction. After reaching a snow layer thickness of $0.03\,\mathrm{m}$, the ground surface energy balance is calculated for the snow-pack itself (Table A2). Variables exchanged based on the snow cover are ground surface temperature, surface thermal conductivity and layer thickness of the layer directly under vegetation. Evaporation flux is subtracted from the snow surface. Top of the canopy wind speed is used to calculate the density of the falling snow. Additionally, snow interception is handled like liquid precipitation interception described in Equation 6.

2.3.4 Interactions between the modules

The vegetation module forms the upper boundary layer of the coupled vegetation-permafrost model and replaces the surface energy balance equation used for common CryoGrid representations. The top of the canopy (TOC) surface energy balance is calculated by the vegetation module based on atmospheric forcing. The forest module numerically solves the energy balance of the ground surface below the canopy defined as

$$S_{\mathrm{in}_{\mathrm{canopy}}} - S_{\mathrm{out}_{\mathrm{ground}}} + L_{\mathrm{in}_{\mathrm{canopy}}} - L_{\mathrm{out}_{\mathrm{ground}}} - Q_{\mathrm{h}_{\mathrm{ground}}} - Q_{\mathrm{e}_{\mathrm{ground}}} - Q_{\mathrm{s}_{\mathrm{ground}}} = 0, \tag{2}$$

https://doi.org/10.5194/bg-2020-201
Preprint. Discussion started: 18 June 2020


Biogeosciences Discussions Open Access EGU

where $L_{\mathrm{in}_{\mathrm{canopy}}}$ and $S_{\mathrm{in}_{\mathrm{canopy}}}$ are the incoming long- and shortwave radiation at the ground surface and the lower boundary fluxes of the multilayer canopy module, and $S_{\mathrm{out}_{\mathrm{ground}}}$ is the outgoing shortwave flux from the ground, $L_{\mathrm{out}_{\mathrm{ground}}}$ the outgoing longwave flux, $Q_{\mathrm{h}_{\mathrm{ground}}}$ the sensible heat flux, $Q_{\mathrm{e}_{\mathrm{ground}}}$ the latent heat flux, and $Q_{\mathrm{s}_{\mathrm{ground}}}$ the storage heat flux at the ground surface. The first six components of the sub-canopy energy balance directly replace the respective components surface energy balance scheme of CryoGrid (Equation 2. Whereas $Q_{\mathrm{s}_{\mathrm{ground}}}$ is calculated based on temperatures of the uppermost ground or snow layers that are passed from CryoGrid to the forest module. The storage heat flux is calculated as

$$Q_{\mathrm{s}_{\mathrm{ground}}} = k\frac{T_{\mathrm{s}} - T_{\mathrm{ground}}}{\Delta z}, \tag{3}$$

where k is the soil thermal conductivity, T_{s} the soil surface temperature, T_{ground} the actual ground temperature for the first layer below the surface and Δz the layer thickness. In Fig. 2 the energy fluxes expected for a forested and a grassland site in the snow-covered and snow-free periods each are illustrated schematically.

https://doi.org/10.5194/bg-2020-201
Preprint. Discussion started: 18 June 2020

Biogeosciences
Discussions
Open Access
EGU

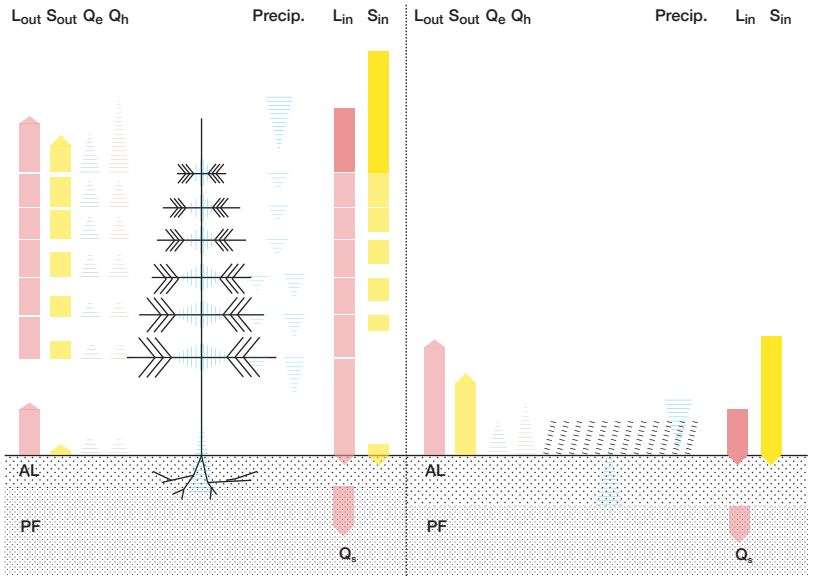

(a)

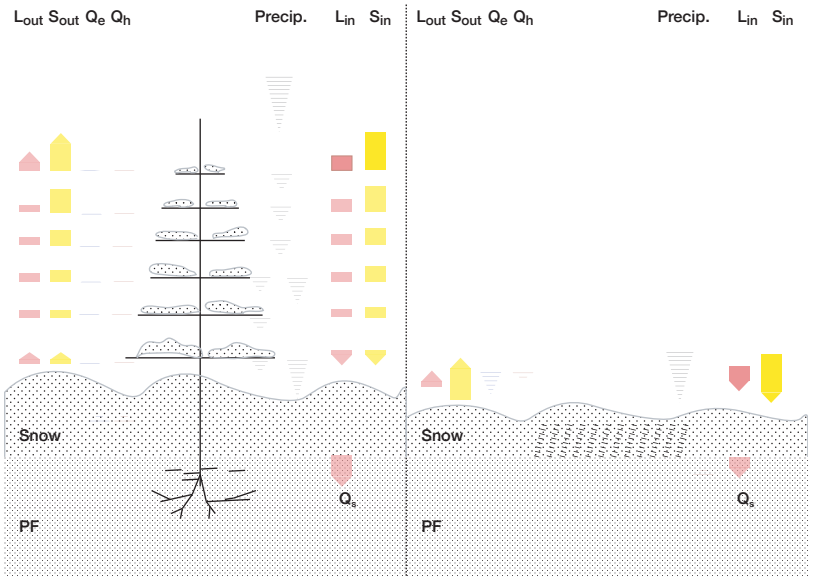

(b)

Figure 2. Schematic of the surface energy and water balance of the forest (left) and grassland (right) schemes for (a) snow-free period and (b) snow-covered period. The active layer (AL), the frozen ground (PF), tree and grassland (dotted lines) and the snow pack (Snow) in the snow covered period. In each of the four panels, incoming and outgoing longwave (L_{in}, L_{out}), incoming and outgoing solar (S_{in}, S_{out}), turbulent fluxes (Q_h and Q_e), the storage heat flux (Q_s), and precipitation (and interception) of rain- and snowfall are shown.

https://doi.org/10.5194/bg-2020-201
Preprint. Discussion started: 18 June 2020


Biogeosciences Discussions Open Access EGU

In the novel model set-up which allows for soil-vegetation interaction, the vegetation module receives ground state variables of the top $0.7\,\mathrm{m}$ of the soil layers. These state variables are soil layer temperature (T_{ground}) and soil layer moisture (W_{ground}), as well as the diagnostic variables soil layer conductivity (k_{ground}), and ice content (I_{ground}). The vegetation transpiration fluxes are subtracted from the ground soil layers within the rooting depth and evaporation fluxes from the ground surface. Following the notation in Bonan et al. (2018) the rain and snow fraction reaching the ground ($W_{\mathrm{ground_s}}$) is described as follows

$$\frac{\delta W_{ground_s}}{\delta t} = fP_R + D_c - E_c + D_t - E_t \tag{4}$$

and consist of the direct throughfall (fP_R), the canopy drip (D_c), the canopy evaporation (E_c), the stemflow (D_t) and the stem evaporation (E_t), which are based on the retained canopy water (W_c)

$$\frac{\delta W_c}{\delta t} = (1 - f - f_t)P_R - E_c - D_c, \tag{5}$$

where $1 - f - f_t P_R$ is the intercepted precipitation, and the retained trunk water (W_t)

$$\frac{\delta W_t}{\delta t} = f_t P_R - E_t - D_t, \tag{6}$$

respectively.

2.4 Model setup and simulations

We run model simulations for forested and non-forested scenarios based on in-situ measurements recorded in 2018 and 2019. The subsurface stratigraphies used in CryoGrid is described by the mineral and organic content, natural porosity, field capacity and initial water/ice content. Some of these parameters could be measured at the forest and grassland sites and were used to set the initial soil profiles in the model. Table A3 summarizes all parameter choices for soil stratigraphies and Table A4 summarizes constants used. The subsurface stratigraphy extends to $100\,\mathrm{m}$ below surface where the geothermal heat flux is set to 0.05 W/m^2 (Langer et al., 2011b). The ground is divided into separate layers in the model. The uppermost $8\,\mathrm{m}$ have a layer thickness of $0.05\,\mathrm{m}$, followed by $0.1\,\mathrm{m}$ for the next $20\,\mathrm{m}$, $0.5\,\mathrm{m}$ up to $50\,\mathrm{m}$ and $1\,\mathrm{m}$ thereafter. The remaining CryoGrid parameters were adopted from previous studies using CryoGrid (Table A2) (Langer et al., 2011a, b, 2016; Westermann et al., 2016; Nitzbon et al., 2019, 2020). We use ground surface temperature (GST) as the target variable for model validation. GST results from the surface energy balance at the interface between canopy, snow cover, and ground and provides an integrative measure of the different model components. In addition it is the most important variable determining the thermal state of permafrost.

For the canopy stratigraphy, we follow the parameterizations in Bonan et al. (2018) for the plant functional type deciduous needleleaf (see Table A5 and A6). This canopy stratigraphy can be described by two parameters: the leaf area index (LAI) measured at the bottom of the canopy defines the total leaf area. The leaf area density function on the other hand describes the

https://doi.org/10.5194/bg-2020-201
Preprint. Discussion started: 18 June 2020

foliage area per unit volume of canopy space which is the vertical distribution of leaf area. Leaf area density is measured by evaluating the amount of leaf area between two heights in the canopy separated by the distance. This function can be expressed by the beta distribution probability density function which provides a continuous representation of leaf area for the use with multilayer models (Bonan (2019) for further information). Here, we use the beta distribution parameters for needleleaf trees (p = 3.5, q = 2) which resembles a cone-like tree shape. LAI can be estimated from satellite data, calculated from below-canopy light measurements or by harvesting leaves and relating their mass to the the canopy diameter. To assess the LAI we use data from literature. Following Kobayashi et al. (2010) who conducted an extensive study using satellite data, the average LAI for our forest type is set to $4\,\mathrm{m}^2/\mathrm{m}^2$ and stem area index (SAI) is set to $0.05\,\mathrm{m}^2/\mathrm{m}^2$, resulting in a plant area index (PAI) of $4.05\,\mathrm{m}^2/\mathrm{m}^2$ and 9 vegetation layers for model simulations. The lower atmospheric boundary layer is simulated by $4\,\mathrm{m}$ of atmospheric layers.

We perform simulations over a 5-year period from August 2014 to August 2019. The model runs are initialized with a typical temperature profile of $0\,\mathrm{m}$ depth: $0\,^\circ\mathrm{C}$, $2\,\mathrm{m}$: $0\,^\circ\mathrm{C}$, $10\,\mathrm{m}$: $-9\,^\circ\mathrm{C}$, $100\,\mathrm{m}$: $5\,^\circ\mathrm{C}$, $5000\,\mathrm{m}$: $20\,^\circ\mathrm{C}$. Spin-up period prior to the validation period is 4 years before we compare modeled and measured data. Test runs with a longer spin up period of 10 years confirmed that only 4 years are sufficient when focusing on GST. The meteorological forcing data required by the model include: air temperature, relative humidity, air pressure, wind speed, liquid and solid precipitation, and incoming short- and longwave radiation. ERA-Interim data for the coordinate N $63.18946°$, E $118.19596°$ were used to obtain forcing data for the total available period from 1979 to 2019 (Simmons et al., 2007).

3 Results

3.1 Model validation and in-situ measurements

The model is validated against ground surface temperature (GST) measurements of forested and non-forested study sites. The data set used covers one complete annual cycle from 10. August 2018 to 10. August 2019. In addition, the model output is compared to radiation, snow depth, conductive heat flux, precipitation and temperature measurements of the AWS at the grassland site. The AWS was set up on 5. August 2018 and taken down on 26. August 2019. Data were recorded continuously, except for 40 days in late May / early June due to a power cut. The mean annual air temperature is measured to be $-7.3\,^\circ\mathrm{C}$ with a maximum temperature of $33.1\,^\circ\mathrm{C}$ and a minimum of $-54.0\,^\circ\mathrm{C}$, and an average relative humidity of 70.5%. Precipitation is $129.8\,\mathrm{mm/year}$ (liquid). The maximum snow height at the grassland site is measured to be $0.5\,\mathrm{m}$ in February and the ground was snow-covered for 181 days from 28. October 2018 - 27. April 2019 (values above $0.05\,\mathrm{m}$ snow height). A quality check of the radiation data revealed partly inconsistent incoming longwave radiation measurements for the time-span of 1. November 2018 - 26. February 2019. During this period it is likely that the sensor is partially covered by snow, making it necessary to discard those measurements from the record. High quality Qnet and LW measurements, thus, only exist for the periods 28. to 30. October 2018 and 27. February 2018 to 27. April 2019. This data gap consequently also limits the period for which Bowen Ratios are calculated and sensible heat fluxes (Q_h) and latent heat fluxes (Q_e) can be derived. The mean annual grassland albedo is 0.35 with an average of 0.30 during the snow-free and 0.48 during the snow-covered season. From December to

https://doi.org/10.5194/bg-2020-201
Preprint. Discussion started: 18 June 2020

February the albedo reaches its highest values with a mean of 0.7. Mean annual GST at $0.07\,\mathrm{m}$ depth is $-2.6\,^{\circ}\mathrm{C}$ (range from $19.1\,^{\circ}\mathrm{C}$ to $-24.9\,^{\circ}\mathrm{C}$) with an average of $-11.4\,^{\circ}\mathrm{C}$ in the snow-covered period and $8.0\,^{\circ}\mathrm{C}$ in the snow-free period. The average annual GST recorded in forested areas at a depth of $0.03\,\mathrm{m}$ is $1.9\,^{\circ}\mathrm{C}$ (range from $15.6\,^{\circ}\mathrm{C}$ to $-23.4\,^{\circ}\mathrm{C}$) with an average of $-9.3\,^{\circ}\mathrm{C}$ in the snow-covered period and $5.6\,^{\circ}\mathrm{C}$ in the snow-free period.

3.1.1 Surface energy balance

In a first step we assess the surface energy balance by comparing the modeled net radiation (Q_{net}), sensible heat flux (Q_h), latent heat flux (Q_e) and the storage heat flux (Q_s) at the forested site and the modeled and measured fluxes at the grassland site (Fig. 3 and Appendix A). Turbulent fluxes at forest ground are close to zero for both snow-free and snow-covered periods. TOC sensible heat flux is highest in snow-free period ($62.0\,\mathrm{W\,m^{-2}}$), resulting in the highest net radiation flux ($89.1\,\mathrm{W\,m^{-2}}$). Latent heat flux in the snow-free period is similar for forest TOC ($15.8\,\mathrm{W\,m^{-2}}$), and grassland (measured ($22.1\,\mathrm{W\,m^{-2}}$) and modeled ($18.5\,\mathrm{W\,m^{-2}}$)). During the snow-covered season forest TOC and ground turbulent heat fluxes and net radiation are close to zero. Net radiation flux in the snow-covered period is smallest at the grassland site (measured ($-18.0\,\mathrm{W\,m^{-2}}$) and modeled ($-20.0\,\mathrm{W\,m^{-2}}$). The resulting storage flux is more than double at the forest ground ($29.2\,\mathrm{W\,m^{-2}}$) for the snow-free period and slightly positive ($1.4\,\mathrm{W\,m^{-2}}$) during the snow-covered period.

https://doi.org/10.5194/bg-2020-201
Preprint. Discussion started: 18 June 2020

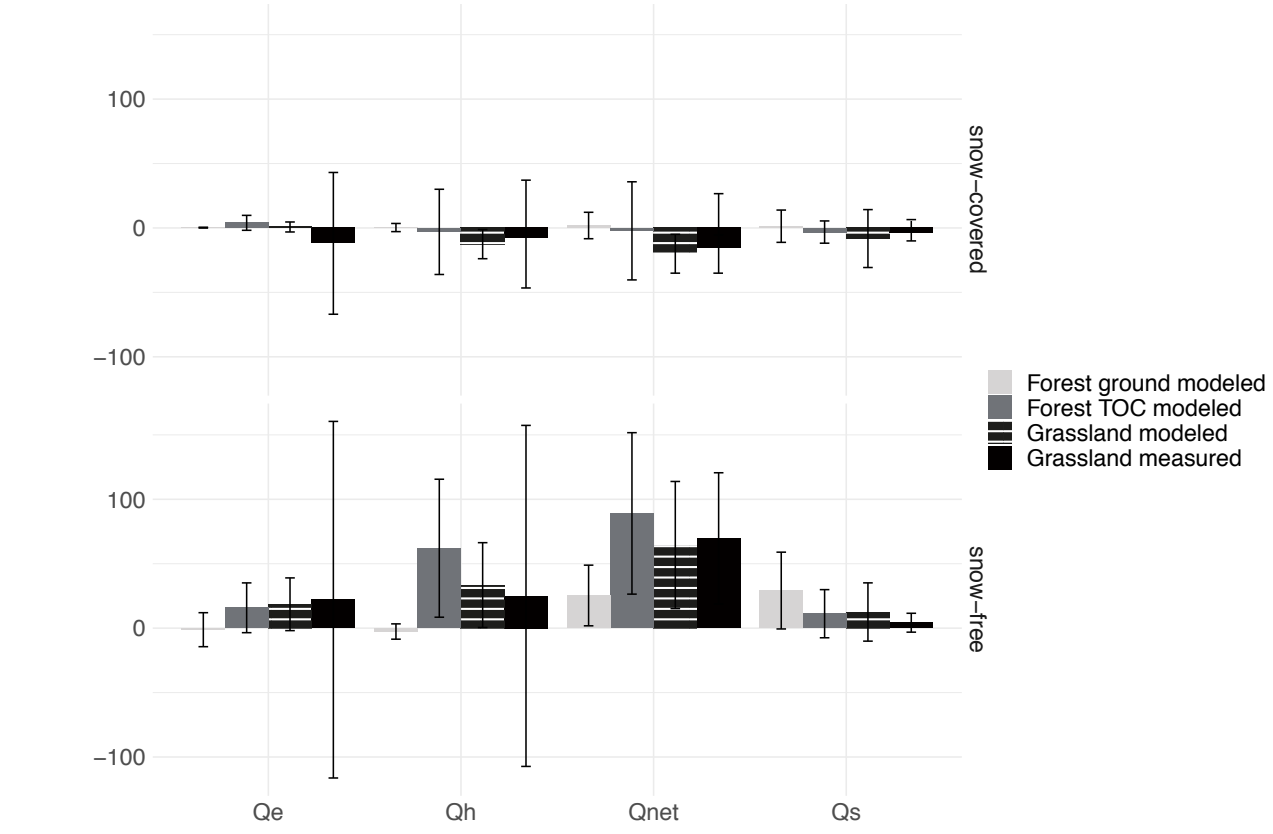

Figure 3. Surface energy balance for snow-covered (28.10.2018-27.04.2019) and snow-free (10.10.2019-27.10.2019 and 28.04.2019-10.10.2019) periods at the ground surface of grassland and forest and at the top of the canopy of forest (Forest TOC). Shown are the net radiation (Q_{net}), sensible (Q_h), latent (Q_e) and storage heat flux (Q_s) for the model runs of the forest and grassland site as well as the measured values at the grassland site.

Average measured Bowen Ratio (B) at the AWS is 1.04, with an average of 1.94 for snow-free and 0.35 for snow-covered periods. At the grassland site the model predicts a B of 1.8 for the snow-free period and -16.54 for the snow-covered period. Which sums up to an annual average B of 1.09 for grassland. Modeled annual average B at the forest ground is more than double with 2.39, 2.19 for the snow-free period and 1.35 for the snow-covered period. Top of canopy modeled annual average B is 2.99, with an average of -0.77 in the snow-covered period and 3.93 in the snow-free period.

More detailed insights into differences of available radiation at the ground surface are presented in Fig. 4. Here, the incoming short- and longwave radiation measured at the grassland site and modeled for the forest and grassland are shown. The longwave radiation dominates the incoming part of the radiation balance at both sites throughout the year. In the snow-free period downward longwave radiation flux is $64.0\,\mathrm{W\,m^{-2}}$ higher at the forest ground. In the snow-covered period downward longwave radiation flux is $39.5\,\mathrm{W\,m^{-2}}$ higher at the forest ground. This results in a surplus of energy under the forest canopy. The shortwave radiation reaching the forest ground is very small for both periods ($14.4\,\mathrm{W\,m^{-2}}$ for snow-free and $3.8\,\mathrm{W\,m^{-2}}$ for

https://doi.org/10.5194/bg-2020-201
Preprint. Discussion started: 18 June 2020

snow-covered periods), showing that the canopy successfully intercepts (absorbs and reflects) most of the incoming shortwave radiation. Snow-free shortwave down at the grassland site is more than 12 times higher in the snow-free period and 16 times higher in the snow-covered-period.

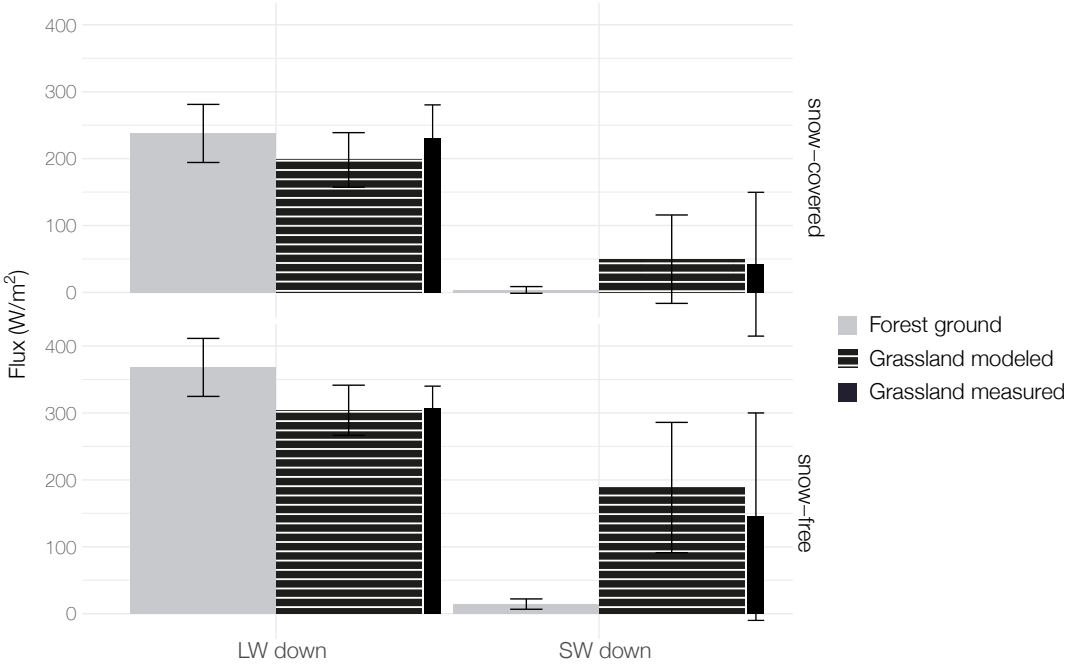

Figure 4. Modeled incoming solar and longwave radiation for snow-covered (28.10.2018-27.04.2019) and snow-free (10.10.2019-27.10.2019 and 28.04.2019-10.10.2019) periods at the ground surface of forest (grey) and grassland (striped). Measured (black) incoming solar (for the same time periods) and longwave radiation (for 28. to 30. October 2018 and 27. February 2018 to 27. April 2019) are shown for the grassland site.

3.1.2 Thermal regime of the ground near the surface

In a second step, we compare the annual, snow-free and snow-covered period average GST to understand the overall model performance and the relative temperature differences between the forest and grassland sites (Fig. 5).

https://doi.org/10.5194/bg-2020-201
Preprint. Discussion started: 18 June 2020

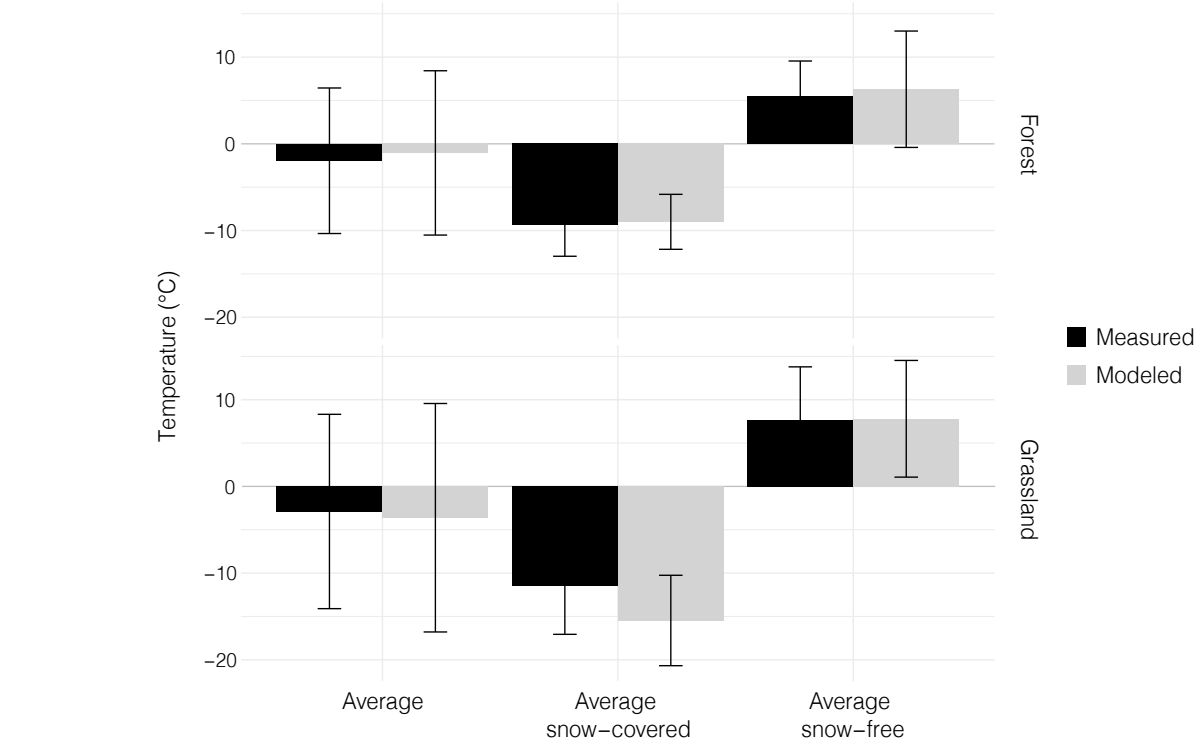

Figure 5. Average measured snow-covered period GST, average measured snow-free period GST, annual average measured GST and the respective standard deviations in forest (top, at $0.03\,\mathrm{m}$ depth) and grassland (bottom, at $0.07\,\mathrm{m}$ depth) over a measurement period of 1 year (10. August 2018 - 10. August 2019).

Measured and modeled average GST values are summarized in Table 2. The highest deviation between modeled and measured GST is found at the grassland site. Here, the model shows a cold bias of $-4.1\,^{\circ}\mathrm{C}$. Also, there is a warm bias of $0.9\,^{\circ}\mathrm{C}$ in the snow-free period in the forest. Overall, we find an average annual difference of $0.9\,^{\circ}\mathrm{C}$ between the two sites. For snow-free season this difference is $2.2\,^{\circ}\mathrm{C}$ and snow-covered $2.1\,^{\circ}\mathrm{C}$, respectively.

Table 2. Measured and modeled ground GST values for both sites.

Site	Time period	Modeled	Measured
Forest	Snow-covered	*-9.0*	*-9.4*
	Snow-free	*6.3*	*5.4*
Grassland	Snow-covered	*-15.5*	*-11.4*
	Snow free	*7.8*	*7.7*

For a more detailed understanding of the annual cycle of the thermal evolution of permafrost ground at our study sites we compare the weekly averaged GST at the grassland and forest site (see Fig. 6). The more detailed analysis of the annual cycle

https://doi.org/10.5194/bg-2020-201
Preprint. Discussion started: 18 June 2020

reveals periods with distinct differences between the model simulation and the measured values. For both study sites the model produces a slight GST overestimation in summer and a prolonged thawing period in spring. The measured data shows a much faster ground warming in spring. This difference is over 20 days at the forest site and 15 days later at the grassland site. In addition, there is a cold bias by $5\,^{\circ}\mathrm{C}$ in January at the grassland site. This bias is not seen at the forest site. Thawing starts later in model simulations than measured.

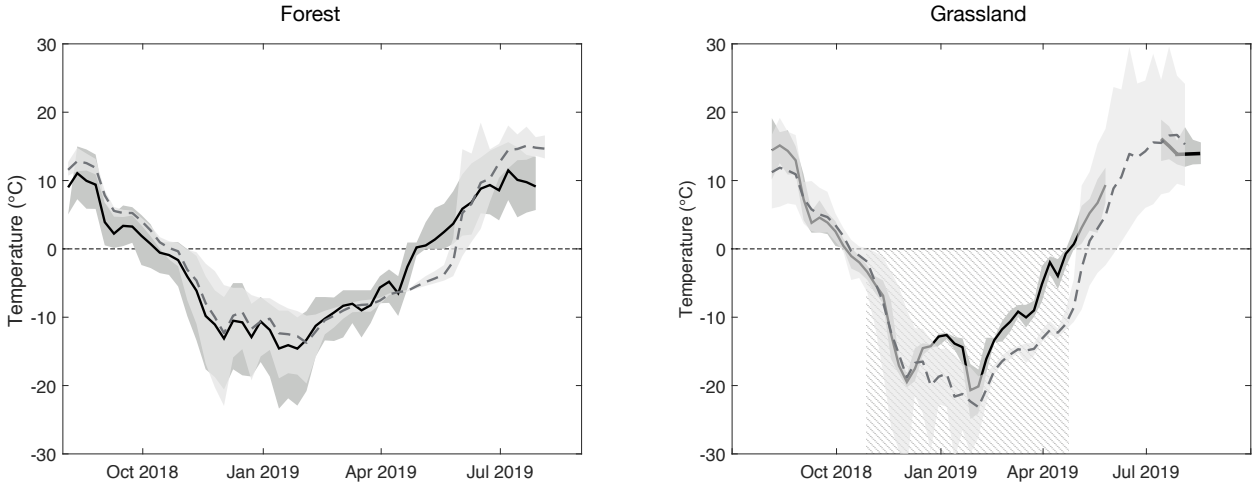

Figure 6. (a) Modeled (grey) and measured (black) average weekly GST in $0.03\,\mathrm{m}$ depth in forest, and (b) in grassland in $0.07\,\mathrm{m}$ depth with standard deviation for modeled (light grey) and measured (dark grey). In addition, the measured duration of the snow-covered period is shaded at the grassland site (b).

To further understand the temporal evolution of the permafrost ground, we compare the modeled and measured active layer thickness at both study sites. In the grassland, the modeled maximum active layer thickness (ALT) is $2.35\,\mathrm{m}$ between 13. and 24. October 2018, complete freezing occurred on the 9th of November and top soil thawing started on the 3rd of May. The measured ALT in the grassland was $2.3\,\mathrm{m}$ in mid-August 2018 and early-August 2019. The measured ALT in the forest was between 0.5 and $1.1\,\mathrm{m}$ in mid-August 2018. In the forest, the modeled maximum ALT is $2.1\,\mathrm{m}$ in October 2018 with complete through-freezing on 2nd of December, 23 days later than in the grassland. Top soil thawing begins on June 1st, 29 days later than in grassland. The modeled ALT in August 2018 is between $1.4\,\mathrm{m}$ and $1.8\,\mathrm{m}$ and therefore overestimated by $0.9\,\mathrm{m}$ compared to the point measurements taken in August 2018. Moreover, the measured volumetric water content (VWC) in grassland reaches its maximum of 0.2 in August. The averaged measured VWC at the forest site in August 2018 was 0.3. The model can broadly reproduce this difference but their is a model bias towards higher VWC for both sites. The modeled maximum water content in forest is 0.5 between the end of June and the beginning of July and is about 0.2 higher than in grassland, where the simulation shows a maximum VWC of 0.3 in August. The modeled winter ice content in grassland reaches a maximum value of 0.36 and 0.42 in forest.

https://doi.org/10.5194/bg-2020-201
Preprint. Discussion started: 18 June 2020

3.1.3 Snow cover assessment

To analyze differences in the snow cover evolution, we compare modeled and measured snow depth at the AWS and the modeled snow depth in forest. Snow depth modeled in grassland agrees well with the measured snow depth and reaches a maximum value of $0.26\,\mathrm{m}$ in late April (see Fig. 7). Towards spring, the snow pack in the forest accumulates to $1.2\,\mathrm{m}$ and snow melting starts around the same period but lasts much longer up until the end of May.

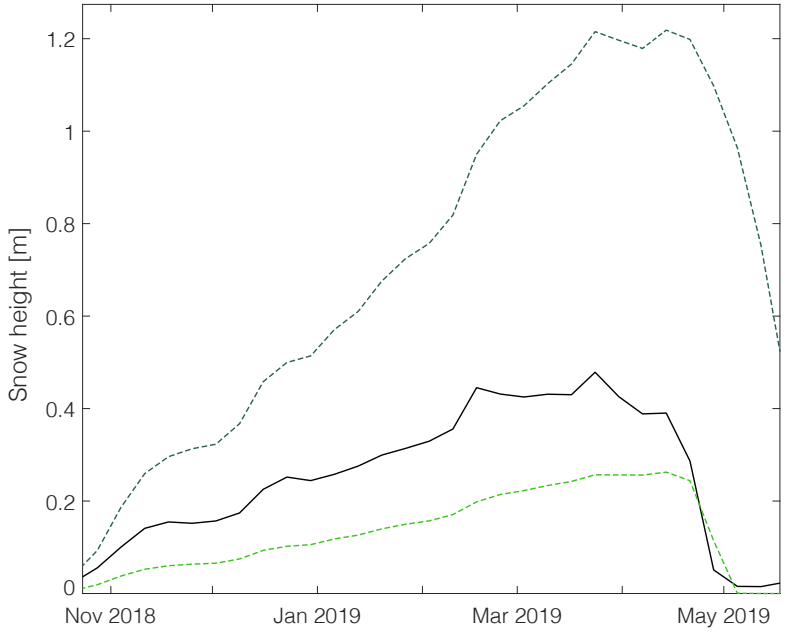

Figure 7. Measured snow depth at AWS (black solid line), modeled snow depth in grassland (light green) and modeled snow depth in forest (dark green)

To understand the high impact that coupling the vegetation has on the snow cover, we next look at the surface energy balance simulated by our model for our specific study site and a hypothetical, sparse canopy with LAI = 1 (see Fig. 8). Incoming solar radiation at the ground is 5 times higher in the sparse canopy simulation, which leads to a higher net radiation flux (Q_{net}) and higher snow melt rates. Turbulent fluxes (Q_h and Q_e) are similar, which suggests that air circulation is blocked, even in a very sparse canopy. The high longwave radiation at the forest ground is persistent for the hypothetical sparse canopy as well, and longwave radiation is still the dominant energy component.

https://doi.org/10.5194/bg-2020-201
Preprint. Discussion started: 18 June 2020

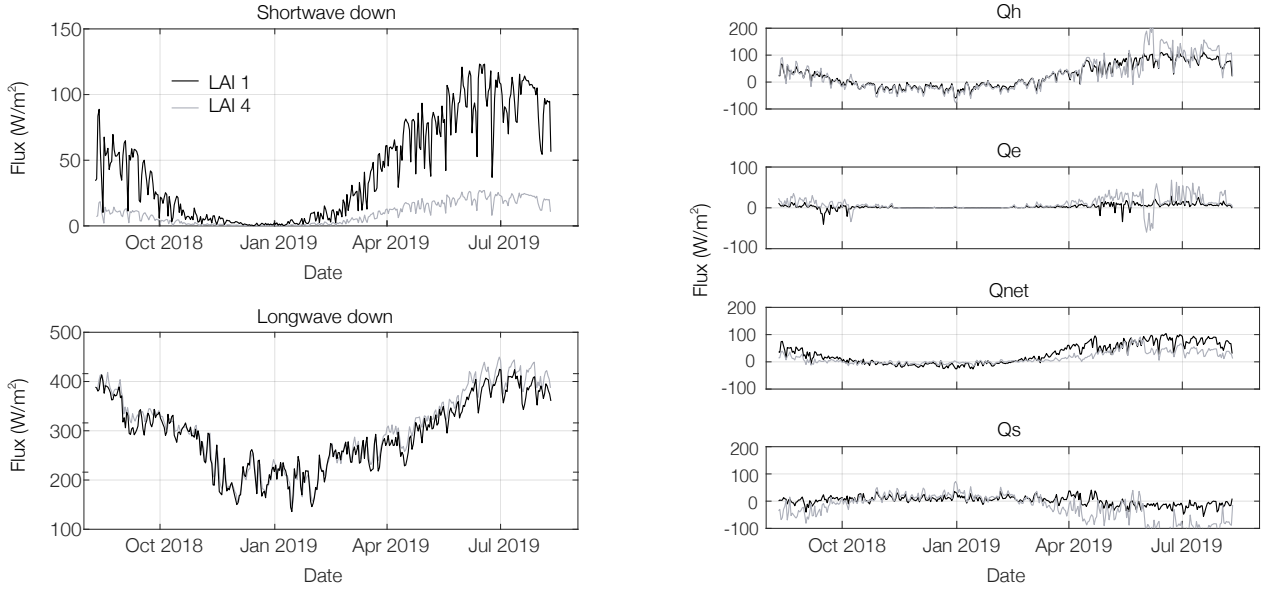

(a) (b)

Figure 8. (a) Modeled longwave and solar radiation at the forest ground for LAI = 1 and LAI = 4 (black) and (b) modeled turbulent fluxes (Q_h and Q_e), net radiation (Q_{net}) and storage heat flux at the forest ground (Q_s).

4 Discussion

The model presented here is found to be capable of simulating the ground thermal regime of permafrost underneath boreal forests. The implemented scheme is able to simulate the physical processes that define the vertical exchange of radiation, heat, water and snow between permafrost and canopy. Our simulations show that the forests exert a strong control on the thermal state of permafrost. At the grassland site, we find a much larger ground surface temperature (GST) amplitude of $60.35\,^{\circ}\mathrm{C}$ over the annual cycle, which is $19\,^{\circ}\mathrm{C}$ higher than at the forest site. This vegetation dampening effect on soil temperature is well-described in literature (Oliver et al., 1987; Balisky and Burton, 1993; Chang et al., 2015). Earlier work by Bonan and Shugart (1989) found that forest soils generally thaw later and less deeply, and are cooler than in open areas. In the winter, forested soils are typically warmer relative to open areas. The tree cover can maintain stable permafrost under otherwise unstable thermal conditions (Bonan and Shugart, 1989). Our results are in agreement with these observations, but further demonstrate that the impact of mixed boreal forest on the GST is strongest during the snow period and the summer peak with the warmest months. Our model reveals an average of $6.5\,^{\circ}\mathrm{C}$ higher GST during the snow-covered period and $1.5\,^{\circ}\mathrm{C}$ lower GST during the snow-free period. Our model simulations unravel that the strong control on the thermal state of permafrost is a result of the combined effects of canopy shading, suppression of turbulent heat fluxes, below-canopy longwave enhancement, increased soil moisture

https://doi.org/10.5194/bg-2020-201
Preprint. Discussion started: 18 June 2020

and distinct snow cover dynamics. These relevant processes controlling forest insulation will be discussed individually in the following subsections. Then, we will present a detailed discussion on the model applicability and limitations of the model.

4.1 Canopy shading and longwave enhancement

The surface energy balances simulated by the model are very different for grassland and forest. The forest canopy reflects and absorbs over 92% of incoming solar radiation for both snow-free and snow-covered periods. The forest ground albedo therefore has little influence on the energy balance. This canopy shading effect makes the longwave radiation the only source of radiative energy at the forest site for both time periods. A surplus of longwave radiation by over 20% is largely trapped below the canopy due to extremely low turbulent heat fluxes, similar to a greenhouse. The increased longwave radiation results in a relatively strong storage heat flux. Despite shading, the storage heat flux at the forest site is similar in magnitude to that simulated at the grassland site. This explains the small difference in the modeled depths of the active layer at both sites. The heat flux plate used for measuring the conductive heat flux at the grassland site is designed for use in mineral soil. Due to a certain amount of organic content in the upper soil layer under- or overestimated heat fluxes are possible (Ochsner et al., 2006). This could explain to some extent the difference between measurements and simulations. We further find, that during the snow-free period, the sensible and latent heat flux at the canopy top are high while being close to zero at the forest ground. In spring, we see a high negative latent heat flux at the forest ground which points at a condensation event. This might be due to a still existing snow layer that suddenly gets exposed to warmer air. Further, in Fig. 8 we see that the greenhouse effect caused by longwave enhancement is similar for a canopy with a much lower LAI and turbulent heat fluxes are also small. In summery, we show that the canopy effectively absorbs and reflects the majority of incoming solar radiation, making canopy shading one of the main controlling mechanisms and that the canopy enhances the longwave radiation the forest ground, because of extremely low turbulent heat fluxes.

4.2 Soil moisture, canopy interception and evapotranspiration

According to the majority of studies, tree growth in permafrost areas is limited by summer air temperatures and available water from snow melt, water accumulated within the soil in the previous year and permafrost thaw water (Kharuk et al., 2015; Sidorova et al., 2007). The amount of precipitation in the eastern Siberian Taiga is characteristically small compared to other areas, therefore it is expected that permafrost plays an important role in the existence of these forests (Sugimoto et al., 2002). Sugimoto et al. (2002) found that plants used rainwater during wet summers, but melt water from permafrost during drought summers. This indicates that permafrost provides the direct source of water for plants in drought summers and retains surplus water in the soil until the next summer. They conclude that if this system is disturbed by future warming, the forest stands might be seriously damaged in severe drought summers (Sugimoto et al., 2002). Our grassland site, which was supposedly forested until the 1950s, has dried up and has a much smaller organic layer and a maximum active layer thickness of 2.30 m. The volumetric water content in forest soil is 10-20% higher despite the same amount of precipitation and a higher evaporative flux during the growing season. This points to the conclusion that permafrost plays an important role in regulating the hydrological conditions in this boreal forest area and holds a certain amount of ground water that is later available to plants.

https://doi.org/10.5194/bg-2020-201
Preprint. Discussion started: 18 June 2020

4.3 Insulating litter and moss layer

The existence of a thick moss and organic layer on the forest ground can significantly lower ground temperatures due to the high insulation impact (Bonan and Shugart, 1989). The low bulk density and low thermal conductivity of the organic mat effectively insulate the mineral soil which causes lower soil temperatures and maintains a high permafrost table. A thick moss-organic layer on the forest floor is an important structural component of boreal forests, controlling energy flow, nutrient cycling, water relations, and through these, stand productivity and dynamics (Bonan and Shugart, 1989). At our forest site the found moss coverage was between 0 and 40% with a thickness from $0.005 - 0.02\,\mathrm{m}$. This is a comparably thin moss layer but was taken into account in the ground set-up for the forest site.

4.4 Snow pack dynamics

Snow cover dynamics on the other hand seem to be a highly important factor in regard to the thermal evolution of the underlying permafrost ground (Gouttevin et al., 2012). Snow cover is an essential component in every ecosystem, acting as a radiation shield, insulator and water reservoir. The forest canopy is also a major contributing factor to differences in snow accumulation. The seasonal snow pack exhibits different characteristics than in the grassland. Snow interception in the canopy, mass unload from the branches to the ground, and sublimation all depend on the canopy structure (Price, 1988). Our simulations further show, an increase in longwave radiation, a decrease in solar flux at the forest ground and the oppression of turbulent fluxes, which all lead to much slower snow melting, less snow compaction, and therefore a much higher snow pack. This is in agreement with earlier work on snow pack modeling in coniferous forests (Price, 1988). For example, Beer et al. (2007) note that these vegetation effects (solar radiation extinction and atmospheric turbulence) have a far greater influence on snow cover dynamics in eastern Siberian boreal forests than snow interception alone. In addition, Grippa et al. (2005) found that leaf area index (LAI) and snow depth are highly connected. We therefore compared the surface energy balances and snow cover dynamics of a very sparse, hypothetical canopy with LAI of 1 to our forest study site with a LAI of 4. As described above, the main difference between the two canopies is seen in the shortwave flux at the forest ground. In a sparse canopy this flux is up to 5 times higher in the snow-free period. Snow depth analysis further reveals that for such as sparse forest the maximum snow depth reaches $0.23\,\mathrm{m}$ only, with a maximum ALT of $0.88\,\mathrm{m}$ and an annual average δT of $0.8\,^{\circ}\mathrm{C}$. This shows that the differences between the thermal development of different forest and grassland sites are highly influenced by the depth, density and the resulting insulation capacities of the snow cover, which is in turn controlled by the canopy density. The LAI of a mature, pure, medium dense larch canopy is around 2.35 for the short growing season and 0 for the rest of the year (Kobayashi et al., 2010). The LAI at our mixed forest site is greater and does not change according to the season. Deciduous larch forests with lower LAI values would lead to lower snow interception values, lower radiation interception and lower suppression of turbulent fluxes, which can explain the very low ALT values found in larch-dominated forest stands. Further, the high snow pack is in accordance with studies of boreal forest snow depths in other boreal regions in Canada (Kershaw and McCulloch, 2007; Fortin et al., 2015). Similar values were also found in a study in mixed boreal forests in Northeastern China (Chang et al., 2015) and in a more general large-scale approach for the circumpolar north (Zhang et al., 2018).

https://doi.org/10.5194/bg-2020-201
Preprint. Discussion started: 18 June 2020

4.5 Applicability and model limitations

The presented model accurately simulates the recorded GST. The detailed analysis of the annual cycle shows that the snow melt period in spring is biased at the forest and grassland sites. In reality, the ground warms up faster than modeled and in the forest this might be due to the high snow cover. Forest snow depth and density measurements would be highly desirable for future work. Further, snow redistribution is not included in our model, but could be an interesting parameter to look at. Additionally, one aspect not represented in the model is the moisture transport and migration in frozen ground or the forming of ice lenses. These processes could lead to the observed, lower ALT at the forest site. Further, actual plant area index values based on collected field data could be incorporated in the future for a more detailed understanding of the exact canopy density, but were out of scope for this particular study. An existing, extensive tree survey data set could be used to calculate the actual plant area indices in the proximity of our study site. A second canopy aspect not considered here, is the reduced leaf area index of deciduous larch stands outside of the comparably short growing season. Based on the ALT point measurements at the forest site it is clear that our model overestimates the ALT in the forest. One feasible explanation is the overestimation of the snow cover which leads to higher winter insulation. This could be due to a missing LAI constraint affecting deciduous taxa in the snow-covered period. The model used here is not particularly parameterized for the application in deciduous larch stands, and we do not have snow depth measurements in the forest. A complete removal of the leaf area mass would lead to higher turbulent fluxes, higher solar radiation, hence higher melt rates and more snow compaction that would potentially counteract the greenhouse effect and snow dynamics described. Our forest site is partly covered by deciduous larch trees (7%), which cause a lower LAI in winter and therefore higher solar radiation before leaf-out in spring. This could change the surface energy balance at the forest ground. In our simulations under a hypothetical, sparse canopy, we find a much lower snow pack height, with a lower insulation effect against the extreme cold and an earlier onset of snow melting processes. In combination, this causes a much lower ALT. To simulate the needle-tossing of deciduous larch, a leaf area index threshold could be incorporated for a certain time period between needle tossing and leaf-out in spring. This tunes the model towards a more detailed representation of highly sensitive larch-dominated forests, which are particular to large parts of Eastern Siberia. This modification could reveal further taxa-specific interactions with permanently frozen ground. It would also be desirable to implement a spatially-explicit, dynamic vegetation model, such as the larch forest simulator (LAVESI, Kruse et al. (2016)) to further analyze the dynamic vegetation distribution under the recognition of the found interactions. This would allow us to simulate the vegetation response to changes in permafrost temperature and hydrology dynamically over a large timescale, and across a wide range of boreal forest ecosystems in Eastern Siberia. In combination, the above model limitations could explain a great part of the GST and ALT differences between measurements and modeled simulations.

5 Conclusions

This study presents a specific application of a coupled multilayer forest-permafrost model to investigate the energy transfer and surface energy balance in permafrost underlain boreal forest of Eastern Siberia. The comparison of measured and modeled GST at a mixed forest and a grassland site, as well as the comparison of the modeled and measured radiation fluxes at the grassland

https://doi.org/10.5194/bg-2020-201
Preprint. Discussion started: 18 June 2020

site, justify the use of the physically-based modeling approach to investigate the thermal regime and surface energy balance in this complex ecosystem. The detailed vegetation model successfully calculates the canopy radiation and water budgets, leaf fluxes, as well as canopy turbulence and aerodynamic conductance. These canopy fluxes alter the below-canopy surface energy balance, the ground thermal conditions and the snow cover dynamics. We find a strong dampening effect of 19 °C on the annual ground surface temperature amplitude of the permafrost. Further, forested permafrost maintains a higher soil water content by controlling water storage in the ground. The forest cover alters the surface energy balance by inhibiting most of the solar radiation and suppressing turbulent heat fluxes. Additionally, we reveal that the canopy leads to a surplus in longwave radiation trapped below the canopy, similar to a greenhouse. Therefore, and despite the canopy shading, the storage heat flux at the forest site is similar in magnitude to that simulated at the grassland site. Further, the end of season snow cover is much greater at the forest site and the onset of the snow melting processes are delayed. In summary, we identify the following key points.

i. The canopy effectively absorbs and reflects over 90% of incoming solar radiation, making canopy shading one of the main controlling mechanisms.

ii. The vegetation cover suppresses the majority of the turbulent heat fluxes in the below-canopy space.

iii. The canopy enhances the longwave radiation below the canopy by up to 20%, similar to a greenhouse, which results in a comparable magnitude of storage heat flux for both sites.

iv. Forested permafrost holds a higher ground water content than the dry grassland site.

v. Canopy shading leads to slower snow melting, less snow compaction, and therefore a higher snow pack.

vi. The differences in the thermal development of the forest and grassland sites are highly influenced by the depth, density and the resulting insulation capacities of the snow cover, which is in turn controlled by the canopy density.

Code and data availability. The code is available at https://github.com/CryoGrid/CryoGrid/tree/vegetation. The iButton soil temperature data are available at https://doi.pangaea.de/10.1594/PANGAEA.915174. The AWS data are submitted to Pangaeae and under review. Temporary files can be accessed here: https://doi.pangaea.de/10.1594/PANGAEA.918074

https://doi.org/10.5194/bg-2020-201
Preprint. Discussion started: 18 June 2020


Biogeosciences Discussions Open Access EGU

Appendix A: Bowen ratio and turbulent heat flux calculation

With the AWS equipped as a Bowen ratio station, B is calculated following (Foken, 2016) as

$$B = \frac{c_p}{L_v} \times \frac{\Delta T}{\Delta q}, \tag{A1}$$

where the specific heat at constant pressure for moist air (c_p) is 1.006 kJ kg^{-1}K^{-1} and the latent heat of vaporization of water (L_v) is 2260 kJ kg^{-1}. With ΔT being the temperature difference between the two air temperature sensors at heights $0.115\,\mathrm{m}$ and $0.252\,\mathrm{m}$. Δq is the difference in specific humidity calculated from measured relative humidity (ϕ), temperature and pressure.

Thereafter, latent heat flux (Q_e) is calculated as

$$Q_e = \frac{Q_s - Q_g}{1 + B}, \tag{A2}$$

and sensible heat flux (Q_h)

$$Q_h = (Q_s - Q_g)\frac{B}{1 + B}, \tag{A3}$$

with the storage heat flux (Q_s)

$$Q_s = L_{in} + S_{in} - L_{out} - S_{out}, \tag{A4}$$

and Q_g as the convective ground heat flux.

https://doi.org/10.5194/bg-2020-201
Preprint. Discussion started: 18 June 2020


Biogeosciences Discussions Open Access EGU

Table A1. Sensors used for field measurements.

Sensor	Brand	Measurement	Accuracy
Temperature and relative humidity probe (HMP155A)	Vaisala	Air temp. / rel. Humidity	$\pm 1\%$ $(15 - 25\,^{\circ}\mathrm{C})$
Alpine wind monitor (05103-45)	R. M. Young C.	Wind speed / direction	1% of reading
Sonic ranging sensor (SR50A)	Campbell	Snow depth	0.4% of height
Barometric sensor (CS100)	Setra	Barometric pressure	± 0.5 mb $(20\,^{\circ}\mathrm{C})$
4-Component Net Radiometer (NR01)	Hukseflux	S/L in and out	10% daily totals
Thermistor probe (107)	Campbell	Soil temperature	$0.2\,^{\circ}\mathrm{C}$
Heat flux sensor (HFP01)	Hukseflux	Ground heat flux	$\pm 3\%$
Raingauge tipping bucket unheated (52203)	R. M. Young C.	Precip. (liquid)	2% up to 25 mm hr^{-1}
Water Content Reflectometer (CS616)	Campbell	Soil moisture	$\pm 2.5\%$ VWC
Hobo 4 Channel Data Logger + Temperaturesensor	Onset	Soil temperature	± 2 mV $\pm 2.5\%$ abs. reading
iButton (DS1922L)	Maxim Integrated	Soil temperature	$\pm 0.5\,^{\circ}\mathrm{C}$ (-10 – $65\,^{\circ}\mathrm{C}$)

https://doi.org/10.5194/bg-2020-201
Preprint. Discussion started: 18 June 2020


Biogeosciences Discussions Open Access EGU

Table A2. Overview of the CryoGrid parameters used

Process / Parameter		Value	Unit	Source
Density falling snow	ρ_{snow}	300	kg m^{-3}	*Kershaw and McCulloch (2007)*
Albedo ground	α	0.3	-	*field measurement*
Roughness length	z_0	0.001	m	*Westermann et al. (2016)*
Roughness length snow	z_{0snow}	0.0001	m	*Boike et al. (2019)*
Geothermal heat flux	F_{lb}	0.05	W m^{-2}	*Westermann et al. (2016)*
Thermal conductivity mineral soil fraction	$k_{mineral}$	3.0	W m^{-1} K^{-1}	*Westermann et al. (2016)*
Emissivity	ϵ	0.99	-	*Langer et al. (2011a)*
Root depth	D_T	0.2	m	*field measurement*
Evaporation depth	D_E	0.1	m	*Nitzbon et al. (2019)*
Hydraulic conductivity	K	10^{-5}	m s^{-1}	*Boike et al. (2019)*

https://doi.org/10.5194/bg-2020-201
Preprint. Discussion started: 18 June 2020


Biogeosciences Discussions Open Access EGU

Table A3. Ground set-up for simulations.

	Top depth	Water/Ice	Mineral	Organic	Field capacity	Natural porosity
Forest	*0*	*0.6*	*0*	*0.2*	*0.5*	*0.8*
	0.08	*0.6*	*0.1*	*0.2*	*0.5*	*0.7*
	0.16	*0.6*	*0.4*	*0*	*0.5*	*0.6*
Grassland	*0*	*0.5*	*0.4*	*0.1*	*0.5*	*0.5*
	0.04	*0.4*	*0.6*	*0*	*0.5*	*0.4*
	0.1	*0.4*	*0.6*	*0*	*0.5*	*0.4*

https://doi.org/10.5194/bg-2020-201
Preprint. Discussion started: 18 June 2020


Biogeosciences Discussions Open Access EGU

Table A4. Constants

Constants	Value	Unit	Source
von Karman	0.4	-	Westermann et al. (2016)
Gravitational acceleration	9.80616	m s^{-2}	Westermann et al. (2016)
Freezing point water (normal pres.)	273.15	K	Westermann et al. (2016)
Latent heat of vaporization	2.501 x 10^6	J kg^{-1}	Westermann et al. (2016)
Molecular mass of water	18.016/1000	kg mol^{-1}	Bonan (2019)
Molecular mass of dry air	28.966/1000	kg mol^{-1}	Bonan (2019)
Specific heat dry air (const. pres.)	1004.64	J kg^{-1} K^{-1}	Bonan (2019)
Density of fresh water	1000	kg m^{-3}	Westermann et al. (2016)
Density of ice	917	kg m^{-3}	Westermann et al. (2016)
Heat of fusion for water at 0 °C	0.334 x 10^6	J kg^{-1}	Westermann et al. (2016)
Stefan-Boltzman constant	5.67 x 10^-8	W m^{-2} K^{-4}	Westermann et al. (2016)
Thermal conductivity of water	0.57	W m^{-1} K^{-1}	Westermann et al. (2016)
Thermal conductivity of ice	2.29	W m^{-1} K^{-1}	Westermann et al. (2016)
Pi	3.14159	-	Bonan (2019)
Kinem. visc. (0 °C, 1013.25 hPa)	0.0000133	m^2 s^{-1}	Bonan (2019)
Mol. diff. (heat) (0 °C, 1013.25 hPa)	0.0000189	m^2 s^{-1}	Bonan (2019)
Mol. diff. (H2O) (0 °C, 1013.25 hPa)	0.0000218	m^2 s^{-1}	Bonan (2019)
Mol. diff. (CO2) (0 °C, 1013.25 hPa)	0.0000138	m^2 s^{-1}	Bonan (2019)
Sp. heat water vapor (const. pr.)	1810	J kg^{-1} K^{-1}	Bonan (2019)
Universal gas constant	8.31446	J K^{-1} $kmole^{-1}$	Bonan (2019)

https://doi.org/10.5194/bg-2020-201
Preprint. Discussion started: 18 June 2020

Table A5. Multilayer canopy parameters

Parameter (PFT NDT boreal)	Value	Unit	Source
Leaf angle dep. from spherical	0.01	-	Bonan (2002)
Leaf reflectance (VIS/NIR)	0.07/0.35	-	Bonan (2002)
Stem reflectance (VIS/NIR)	0.16/0.39	-	Bonan (2002)
Leaf transmittance (VIS/NIR)	0.05/0.01	-	Bonan (2002)
Stem transmittance (VIS/NIR)	0.001/0.001	-	Bonan (2002)
Maximum carboxylation rate (25 °C)	43	umol m^{-2} s^{-1}	Bonan (2002)
Photosynthetic pathway	C3	-	Bonan (2002)
Leaf emissivity	0.98	-	Bonan (2002)
Quantum efficiency a	0.06	umol CO_2 umol $photon^{-1}$	Bonan (2002)
Slope m	6	-	Bonan (2002)
Leaf dimension	0.04	m	Bonan (2002)
Roughness length	0.055	m	Bonan (2002)
Displacement height	0.67	m	Bonan (2002)
Root distribution (a/b)	7.0/2.0	-	Bonan (2002)
Min. vapor pressure deficit	100	Pa	Bonan (2019)
Plant capacitance	2500	mmol H_2O m^{-2} leaf area MPa^{-1}	Bonan (2019)
Minimum leaf water potential	-2	MPa	Bonan (2019)
Stem hydraulic conductance	4	mmol H_2O m^{-2} leaf area s^{-1} MPa^{-1}	Bonan (2019)
Atmospheric CO2	380	umol mol^{-1}	Bonan (2019)
Atmospheric O2	209	mmol mol^{-1}	Bonan (2019)
Soil evaporative resistance	3361.509	s m^{-1}	Bonan (2019)
Specific heat of dry-wet soil	1396	J kg^{-1} K^{-1}	Oleson et al. (2013)
Specific heat of fresh H2O	4188	J kg^{-1} K^{-1}	Oleson et al. (2013)
Specific leaf area at top of canopy	0.01	m^2 g^{-1} C	Bonan et al. (2018)
Fine root biomass	500	g biomass m^{-2}	Bonan (2019)
Leaf drag coefficient	0.25	-	Bonan (2019)
Foliage clumping index	0.7	-	Bonan (2019)

https://doi.org/10.5194/bg-2020-201
Preprint. Discussion started: 18 June 2020


Biogeosciences Discussions Open Access EGU

Table A6. Further ground parameters needed by the vegetation

Soil parameters (Sandy clay loam)	Value	Unit	Source
Soil layer hydraulic cond. at sat.	CryoGrid	mm H2O s^{-1}	Bonan (2019)
Soil layer Clapp Hornberger "b"	4.05 / 4.38 / 10.4	-	Bonan (2019)
Soil water at saturation	CryoGrid	m^3 m^{-3}	Bonan (2019)
Alpha	0.059	m	Bonan (2019)
n	1.48	-	Bonan (2019)
Owr	CryoGrid	m^3 m^{-3}	Bonan (2019)
Ow	VWC	m^3 m^{-3}	Bonan (2019)
Ows	0	-	Bonan (2019)
Water fraction (initialization only)	0.2	-	This study
Root fraction	0.5 / 0.25 / 0.25	-	This study
Volumetric water content	CryoGrid	m^3 m^{-3}	This study
Thermal conductivity	CryoGrid	W m^{-1} K^{-1}	This study
Soil temperature	CryoGrid	K	This study
Soil layer depth / thickness	0.1 /0.1 / 0.7	m	This study
Interface depth	0.05 / 0.15 / 0.45	m	This study
Number of soil layers	3	-	This study

https://doi.org/10.5194/bg-2020-201
Preprint. Discussion started: 18 June 2020

Author contributions. SMS designed the study, carried out the simulations, and wrote the paper. SMS, ML, and TSvD implemented the code in the model. SMS and ML designed the model simulations. SMS, UH and SK conducted the field work in 2018, SMS conducted the field work in 2019. SMS wrote the paper with contributions from all co-authors. UH, ML and JB secured funding.

Competing interests. No competing interests are present.

Acknowledgements. SMS is thankful to the POLMAR graduate school, the Geo.X Young Academy and the WiNS program at the Humboldt University of Berlin for providing a supportive framework for her PhD project and helpful courses on scientific writing and project management. Further, SMS is very grateful for the help during fieldwork in 2018 and 2019, especially for the help from Levina Sardana Nikolaevna, Alexey Nikolajewitsch, Lena Ushnizkaya, Luise Schulte, Frederic Brieger, Stuart Vyse, Elisbeth Dietze, Nadine Bernhard, Boris K. Biskaborn, Iuliia Shevtsova, as well as my co-authors Ljudmila Pestryakova and Evgenii Zakharov. Additionally, SMS would like to thank Stephan Jacobi, Alexander Oehme, Niko Borneman, Peter Schreiber and my co-author William Cable for their help in preparing for field work and the entire PermaRisk and Sparc research groups for their ongoing support.

This study has been supported by the ERC consolidator grant Glacial Legacy of Ulrike Herzschuh (grant no. 772852). Further, the work was supported by the Federal Ministry of Education and Research (BMBF) of Germany through a grant to Moritz Langer (no. 01LN1709A).

https://doi.org/10.5194/bg-2020-201
Preprint. Discussion started: 18 June 2020

References

ACIA: Arctic Climate Impact Assessment. ACIA overview report, http://www.amap.no/documents/doc/arctic-arctic-climate-impact-assessment/796, 2005.

AMAP: Arctic Monitoring and Assessment Program 2011: Mercury in the Arctic, https://doi.org/10.1017/CBO9781107415324.004, http://www.grida.no/amap, 2011.

Balisky, A. C. and Burton, P. J.: Distinction of soil thermal regimes under various experimental vegetation covers, Canadian Journal of Soil Science, 73, 411–420, https://doi.org/10.4141/CJSS93043, 1993.

Beer, C., Lucht, W., Gerten, D., Thonicke, K., and Schmullius, C.: Effects of soil freezing and thawing on vegetation carbon density in Siberia: A modeling analysis with the Lund-Potsdam-Jena Dynamic Global Vegetation Model (LPJ-DGVM), Global Biochemical Cycles, 21, https://doi.org/10.1029/2006GB002760, https://www.bgc-jena.mpg.de/bgi/uploads/Publications/Overview/Beer{_}etal{_}2007.pdf, 2007.

Biskaborn, B. K., Smith, S. L., Noetzli, J., Matthes, H., Vieira, G., Streletskiy, D. A., Schoeneich, P., Romanovsky, V. E., Lewkowicz, A. G., Abramov, A., Allard, M., Boike, J., Cable, W. L., Christiansen, H. H., Delaloye, R., Diekmann, B., Drozdov, D., Etzelmüller, B., Grosse, G., Guglielmin, M., Ingeman-Nielsen, T., Isaksen, K., Ishikawa, M., Johansson, M., Johannsson, H., Joo, A., Kaverin, D., Kholodov, A., Konstantinov, P., Kröger, T., Lambiel, C., Lanckman, J. P., Luo, D., Malkova, G., Meiklejohn, I., Moskalenko, N., Oliva, M., Phillips, M., Ramos, M., Sannel, A. B. K., Sergeev, D., Seybold, C., Skryabin, P., Vasiliev, A., Wu, Q., Yoshikawa, K., Zheleznyak, M., and Lantuit, H.: Permafrost is warming at a global scale, Nature Communications, 10, 1–11, https://doi.org/10.1038/s41467-018-08240-4, 2019.

Boike, J., Nitzbon, J., Anders, K., Grigoriev, M., Bolshiyanov, D., Langer, M., Lange, S., Bornemann, N., Morgenstern, A., Schreiber, P., Wille, C., Chadburn, S., Gouttevin, I., Burke, E., and Kutzbach, L.: A 16-year record (2002-2017) of permafrost, active-layer, and meteorological conditions at the Samoylov Island Arctic permafrost research site, Lena River delta, northern Siberia: an opportunity to validate remote-sensing data and land surface, snow, and , Earth Syst. Sci. Data, 11, 261–299, https://doi.org/10.5194/essd-11-261-2019, https://doi.org/10.5194/essd-11-261-2019, 2019.

Bonan, G. B.: Ecological climatology: concepts and applications, Cambridge University Press, Cambridge, UK, 2002.

Bonan, G. B.: Climate Change and Terrestrial Ecosystem Modeling, Cambridge University Press, https://doi.org/10.1017/9781107339217, 2019.

Bonan, G. B. and Shugart, H. H.: Environmental Factors and Ecological Processes in Boreal Forests, Tech. rep., www.annualreviews.org, 1989.

Bonan, G. B., Williams, M., Fisher, R. A., and Oleson, K. W.: Modeling stomatal conductance in the earth system: Linking leaf water-use efficiency and water transport along the soil-plant-atmosphere continuum, Geoscientific Model Development, 7, 2193–2222, https://doi.org/10.5194/gmd-7-2193-2014, 2014.

Bonan, G. B., Patton, E. G., Harman, I. N., Oleson, K. W., Finnigan, J. J., Lu, Y., and Burakowski, E. A.: Modeling canopy-induced turbulence in the Earth system: A unified parameterization of turbulent exchange within plant canopies and the roughness sublayer (CLM-ml v0), Geoscientific Model Development, 11, 1467–1496, https://doi.org/10.5194/gmd-11-1467-2018, 2018.

Chadburn, S. E., Burke, E. J., Essery, R. L., Boike, J., Langer, M., Heikenfeld, M., Cox, P. M., and Friedlingstein, P.: Impact of model developments on present and future simulations of permafrost in a global land-surface model, Cryosphere, 9, 1505–1521, https://doi.org/10.5194/tc-9-1505-2015, 2015.

https://doi.org/10.5194/bg-2020-201
Preprint. Discussion started: 18 June 2020

Chang, X., Jin, H., Zhang, Y., He, R., Luo, D., Wang, Y., Lü, L., and Zhang, Q.: Thermal Impacts of Boreal Forest Vegetation on Active Layer and Permafrost Soils in Northern da Xing'Anling (Hinggan) Mountains, Northeast China, Arctic, Antarctic, and Alpine Research, 47, 267–279, https://doi.org/10.1657/AAAR00C-14-016, https://www.tandfonline.com/action/journalInformation?journalCode=uaar20, 2015.

Chapin, F. S., Matson, P. A., and Vitousek, P. M.: Earth's Climate System, in: Principles of Terrestrial Ecosystem Ecology, pp. 23–62, Springer, New York, NY, https://doi.org/10.1007/978-1-4419-9504-9_2, http://link.springer.com/10.1007/978-1-4419-9504-9{_}2, 2011.

Chen, Y., Ryder, J., Bastrikov, V., McGrath, M. J., Naudts, K., Otto, J., Ottlé, C., Peylin, P., Polcher, J., Valade, A., Black, A., Elbers, J. A., Moors, E., Foken, T., van Gorsel, E., Haverd, V., Heinesch, B., Tiedemann, F., Knohl, A., Launiainen, S., Loustau, D., Ogée, J., Vessala, T., and Luyssaert, S.: Evaluating the performance of land surface model ORCHIDEE-CAN v1.0 on water and energy flux estimation with a single- and multi-layer energy budget scheme, Geoscientific Model Development, 9, 2951–2972, https://doi.org/10.5194/gmd-9-2951-2016, https://www.geosci-model-dev.net/9/2951/2016/, 2016.

Foken, T.: Angewandte Meteorologie - Mikrometeorologische Methoden, Springer Spektrum, Berlin Heidelberg, 3rd edn., https://doi.org/10.1007/978-3-662-05743-8_8, 2016.

Fortin, V., Jean, M., Brown, R., and Payette, S.: Predicting Snow Depth in a Forest-Tundra Landscape using a Conceptual Model Allowing for Snow Redistribution and Constrained by Observations from a Digital Camera, Atmosphere-Ocean, 53, 200–211, https://doi.org/10.1080/07055900.2015.1022708, https://www.tandfonline.com/action/journalInformation?journalCode=tato20, 2015.

Furyaev, V., Vaganov, E., Tchebakova, N., and Valendik, E.: Effects of Fire and Climate on Successions and Structural Changes in The Siberian Boreal Forest, Eurasian Journal of Forest Research, 2, 1–15, 2001.

Gauthier, S., Bernier, P., Kuuluvainen, T., Shvidenko, A. Z., and Schepaschenko, D. G.: Boreal forest health and global change, Science, 349, 819–822, https://doi.org/10.1126/science.aaa9092, 2015.

Gouttevin, I., Menegoz, M., Dominé, F., Krinner, G., Koven, C., Ciais, P., Tarnocai, C., and Boike, J.: How the insulating properties of snow affect soil carbon distribution in the continental pan-Arctic area, Journal of Geophysical Research: Biogeosciences, 117, 1–11, https://doi.org/10.1029/2011JG001916, 2012.

Grippa, M., Kergoat, L., Le Toan, T., Mognard, N. M., Delbart, N., L'Hermitte, J., and Vicente-Serrano, S. M.: The impact of snow depth and snowmelt on the vegetation variability over central Siberia, Geophysical Research Letters, 32, L21 412, https://doi.org/10.1029/2005GL024286, http://doi.wiley.com/10.1029/2005GL024286, 2005.

Harris, I., Jones, P., Osborn, T., and Lister, D.: Updated high-resolution grids of monthly climatic observations - the CRU TS3.10 Dataset, International Journal of Climatology, 34, 623–642, https://doi.org/10.1002/joc.3711, http://doi.wiley.com/10.1002/joc.3711, 2014.

Hayasaka, H.: Recent Vegetation Fire Incidence in Russia, Global Environmental Research, 15, 5–13, 2011.

Helbig, M., Pappas, C., and Sonnentag, O.: Permafrost thaw and wildfire: Equally important drivers of boreal tree cover changes in the Taiga Plains, Canada, Geophysical Research Letters, 43, 1598–1606, https://doi.org/10.1002/2015GL067193, http://doi.wiley.com/10.1002/2015GL067193, 2016.

Holtmeier, F. K. and Broll, G.: Sensitivity and response of northern hemisphere altitudinal and polar treelines to environmental change at landscape and local scales, Global Ecology and Biogeography, 14, 395–410, https://doi.org/10.1111/j.1466-822X.2005.00168.x, 2005.

IPCC: IPCC: Climate Change 2014 Synthesis Report. Contribution of Working Groups I, II and III to the Fifth Assessment Report of the Intergovernmental Panel on Climate Change, IPCC, Geneva, Switzerland, http://ar5-syr.ipcc.ch/ipcc/ipcc/resources/pdf/IPCC{_}SynthesisReport.pdf, 2014.

IPCC: Summary for Policymakers. In: IPCC Special Report on the Ocean and Cryosphere in a Changing Climate, IPCC, 2019.

https://doi.org/10.5194/bg-2020-201
Preprint. Discussion started: 18 June 2020

Ju, J. and Masek, J. G.: The vegetation greenness trend in Canada and US Alaska from 1984-2012 Landsat data, Remote Sensing of Environment, 176, 1–16, https://doi.org/10.1016/j.rse.2016.01.001, http://dx.doi.org/10.1016/j.rse.2016.01.001, 2016.

Kershaw, G. P. and McCulloch, J.: Midwinter Snowpack Variation Across the Arctic Treeline, Churchill, Manitoba, Canada, Arctic, Antarctic, and Alpine Research, 39, 9–15, https://doi.org/10.1657/1523-0430(2007)39[9:MSVATA]2.0.CO;2, 2007.

Kharuk, V. I., Ranson, K. J., Im, S. T., and Petrov, I. A.: Climate-induced larch growth response within the central Siberian permafrost zone, Environmental Research Letters, 10, https://doi.org/10.1088/1748-9326/10/12/125009, 2015.

Kharuk, V. I., Ranson, K. J., Petrov, I. A., Dvinskaya, M. L., Im, S. T., and Golyukov, A. S.: Larch (Larix dahurica Turcz) growth response to climate change in the Siberian permafrost zone, Regional Environmental Change, 19, 233–243, https://doi.org/10.1007/s10113-018-1401-z, 2019.

Kobayashi, H., Delbart, N., Suzuki, R., and Kushida, K.: A satellite-based method for monitoring seasonality in the overstory leaf area index of Siberian larch forest, Journal of Geophysical Research: Biogeosciences, 115, 1–14, https://doi.org/10.1029/2009JG000939, 2010.

Kruse, S., Wieczorek, M., Jeltsch, F., and Herzschuh, U.: Treeline dynamics in Siberia under changing climates as inferred from an individual-based model for Larix, Ecological Modelling, 338, 101–121, https://doi.org/10.1016/j.ecolmodel.2016.08.003, http://dx.doi.org/10.1016/j.ecolmodel.2016.08.003, 2016.

Langer, M., Westermann, S., Muster, S., Piel, K., and Boike, J.: The surface energy balance of a polygonal tundra site in northern Siberia - Part 1: Spring to fall, Cryosphere, 5, 151–171, https://doi.org/10.5194/tc-5-509-2011, 2011a.

Langer, M., Westermann, S., Muster, S., Piel, K., and Boike, J.: The surface energy balance of a polygonal tundra site in northern Siberia - Part 2: Winter, Cryosphere, 5, 509–524, https://doi.org/10.5194/tc-5-509-2011, 2011b.

Langer, M., Westermann, S., Boike, J., Kirillin, G., Grosse, G., Peng, S., and Krinner, G.: Rapid degradation of permafrost underneath waterbodies in tundra landscapes—Toward a representation of thermokarst in land surface models, Journal of Geophysical Research: Earth Surface, 121, 2446–2470, https://doi.org/10.1002/2016JF003956, 2016.

Loranty, M. M., Abbott, B. W., Blok, D., Douglas, T. A., Epstein, H. E., Forbes, B. C., Jones, B. M., Kholodov, A. L., Kropp, H., Malhotra, A., Mamet, S. D., Myers-Smith, I. H., Natali, S. M., O'donnell, J. A., Phoenix, G. K., Rocha, A. V., Sonnentag, O., Tape, K. D., and Walker, D. A.: Reviews and syntheses: Changing ecosystem influences on soil thermal regimes in northern high-latitude permafrost regions, Biogeosciences, 15, 5287–5313, https://doi.org/10.5194/bg-15-5287-2018, https://doi.org/10.5194/bg-15-5287-2018, 2018.

Nitzbon, J., Langer, M., Westermann, S., Martin, L., Aas, K. S., and Boike, J.: Pathways of ice-wedge degradation in polygonal tundra under different hydrological conditions, Cryosphere, 13, 1089–1123, https://doi.org/10.5194/tc-13-1089-2019, 2019.

Nitzbon, J., Westermann, S., Langer, M., Martin, L. C. P., Strauss, J., Laboor, S., and Boike, J.: Fast response of cold ice-rich permafrost in northeast Siberia to a warming climate, Nature Communications, 11, https://doi.org/10.1038/s41467-020-15725-8, https://doi.org/10.1038/s41467-020-15725-8, 2020.

Ochsner, T. E., Sauer, T. J., and Horton, R.: Field tests of the soil heat flux plate method and some alternatives, Agronomy Journal, 98, 1005–1014, https://doi.org/10.2134/agronj2005.0249, 2006.

Ohta, T., Hiyama, T., Tanaka, H., Kuwada, T., Maximov, T. C., Ohata, T., and Fukushima, Y.: Seasonal variation in the energy and water exchanges above and below a larch forest in eastern Siberia, Hydrological Processes, 15, 1459–1476, https://doi.org/10.1002/hyp.219, 2001.

Oleson, K. W., Lead, D. M. L., Bonan, G. B., Drewniak, B., Huang, M., Koven, C. D., Levis, S., Li, F., Riley, W. J., Subin, Z. M., Swenson, S. C., Thornton, P. E., Bozbiyik, A., Fisher, R., Heald, C. L., Kluzek, E., Lamarque, J.-F., Lawrence, P. J., Leung, L. R., Lipscomb,

W., Muszala, S., Ricciuto, D. M., Sacks, W., Sun, Y., Tang, J., and Yang, Z.-L.: NCAR/TN-503+STR NCAR Technical Note Technical Description of version 4.5 of the Community Land Model (CLM), Tech. rep., http://library.ucar.edu/research/publish-technote, 2013.

Oliver, S. A., Oliver, H. R., Wallace, J. S., and Roberts, A. M.: Soil heat flux and temperature variation with vegetation, soil type and climate, Agricultural and Forest Meteorology, 39, 257–269, https://doi.org/10.1016/0168-1923(87)90042-6, 1987.

Pearson, R. G., Phillips, S. J., Loranty, M. M., Beck, P. S., Damoulas, T., Knight, S. J., and Goetz, S. J.: Shifts in Arctic vegetation and associated feedbacks under climate change, Nature Climate Change, 3, 673–677, https://doi.org/10.1038/nclimate1858, 2013.

Price, A. G.: Prediction of Snowmelt Rates in a Deciduous Forest, Journal of Hydrology, 101, 145–157, 1988.

Rogers, B. M., Soja, A. J., Goulden, M. L., and Randerson, J. T.: Influence of tree species on continental differences in boreal fires and climate feedbacks, Nature Geoscience, 8, 228–234, https://doi.org/10.1038/ngeo2352, 2015.

Romanovsky, V., Smith, S., Shiklomanov, N., Streletskiy, D., Isaksen, K., Kholodov, A., Christiansen, H., Drozdov, D., Malkova, G., and Marchenko, S.: Terrestrial Permafrost in State of the Climate in 2016, Bull Am Meteorol Soc, 98, 147–149, https://doi.org/10.1175/2017BAMSStateoftheClimate.1, 2017.

Ryder, J., Polcher, J., Peylin, P., Ottlé, C., Chen, Y., van Gorsel, E., Haverd, V., McGrath, M. J., Naudts, K., Otto, J., Valade, A., and Luyssaert, S.: A multi-layer land surface energy budget model for implicit coupling with global atmospheric simulations, Geoscientific Model Development, 9, 223–245, https://doi.org/10.5194/gmd-9-223-2016, https://www.geosci-model-dev.net/9/223/2016/, 2016.

Sato, H., Kobayashi, H., Iwahana, G., and Ohta, T.: Endurance of larch forest ecosystems in eastern Siberia under warming trends, Ecology and Evolution, 6, 5690–5704, https://doi.org/10.1002/ece3.2285, 2016.

Scheffer, M., Hirota, M., Holmgren, M., Van Nes, E. H., and Chapin, F. S.: Thresholds for boreal biome transitions, Proceedings of the National Academy of Sciences of the United States of America, 109, 21 384–21 389, https://doi.org/10.1073/pnas.1219844110, 2012.

Schneider Von Deimling, T., Meinshausen, M., Levermann, A., Huber, V., Frieler, K., Lawrence, D. M., and Brovkin, V.: Estimating the near-surface permafrost-carbon feedback on global warming, Biogeosciences, 9, 649–665, https://doi.org/10.5194/bg-9-649-2012, 2012.

Sidorova, O. V., Vaganov, E. A., Naurzbaev, M. M., Shishov, V. V., and Hughes, M. K.: Regional features of the radial growth of larch in north central Siberia according to millennial tree-ring chronologies, Russian Journal of Ecology, 38, 90–93, https://doi.org/10.1134/S106741360702004X, 2007.

Simmons, A., Uppala, S., Dee, D., and Kobayashi, S.: ERA-Interim: New ECMWF reanalysis 20 products from 1989 onwards, Tech. rep., ECMWF Newsletter, 110, https://doi.org/10.21957/pocnex23c6, https://www.ecmwf.int/sites/default/files/elibrary/2007/17713-era-interim-new-ecmwf-reanalysis-products-1989-onwards.pdf, 2007.

Stuenzi, S. M. and Schaepman-Strub, G.: Vegetation Trajectories and Shortwave Radiative Forcing following Boreal Forest Disturbance in Eastern Siberia, Journal of Geophysical Research: Biogeosciences, https://doi.org/10.1029/2019jg005395, 2020.

Sugimoto, A., Yanagisawa, N., Naito, D., Fujita, N., and Maximov, T. C.: Importance of permafrost as a source of water for plants in east Siberian taiga, Ecological Research, 17, 493–503, https://doi.org/10.1046/j.1440-1703.2002.00506.x, http://doi.wiley.com/10.1046/j.1440-1703.2002.00506.x, 2002.

Tchebakova, N. M., Parfenova, E., and Soja, A. J.: The effects of climate, permafrost and fire on vegetation change in Siberia in a changing climate, Environmental Research Letters, 4, https://doi.org/10.1088/1748-9326/4/4/045013, 2009.

Vionnet, V., Brun, E., Morin, S., Boone, A., Faroux, S., Le Moigne, P., Martin, E., and Willemet, J.-M.: The detailed snowpack scheme Crocus and its implementation in SURFEX v7.2, Geoscientific Model Development, 5, 773–791, https://doi.org/10.5194/gmd-5-773-2012, www.geosci-model-dev.net/5/773/2012/, 2012.

https://doi.org/10.5194/bg-2020-201
Preprint. Discussion started: 18 June 2020

Vitt, D. H., Halsey, L. A., Bauer, I. E., and Campbell, C.: Spatial and temporal trends in carbon storage of peatlands of continental western Canada through the Holocene, Canadian Journal of Earth Sciences, 37, 683–693, https://doi.org/10.1139/e99-097, http://www.nrcresearchpress.com/doi/10.1139/e99-097, 2000.

Westermann, S., Langer, M., Boike, J., Heikenfeld, M., Peter, M., Etzelmüller, B., and Krinner, G.: Simulating the thermal regime and thaw processes of ice-rich permafrost ground with the land-surface model CryoGrid 3, Geoscientific Model Development, 9, 523–546, https://doi.org/10.5194/gmd-9-523-2016, 2016.

Zhang, N., Yasunari, T., and Ohta, T.: Dynamics of the larch taiga-permafrost coupled system in Siberia under climate change, Environmental Research Letters, 6, https://doi.org/10.1088/1748-9326/6/2/024003, 2011.

Zhang, Y., Chen, W., and Cihlar, J.: A process-based model for quantifying the impact of climate change on permafrost thermal regimes, Journal of Geophysical Research D: Atmospheres, 108, https://doi.org/10.1029/2002JD003354, 2003.

Zhang, Y., Sherstiukov, A. B., Qian, B., Kokelj, S. V., and Lantz, T. C.: Impacts of snow on soil temperature observed across the circumpolar north, Environmental Research Letters, 13, https://doi.org/10.1088/1748-9326/aab1e7, 2018.

Zweigel, R., Westermann, S., Nitzbon, J., Langer, M., Boike, J., Etzelmüller, B., and Schuler, T. V.: Simulating snow redistribution and its effect on the ground thermal regime at a high-Arctic site on Svalbard, Submitted to: Journal of Geophysical Research - Earth Surface (Manuscript #2020JF005673), 2020.